DESIGN FOR MANUFACTURABILITY OF SPEED-REDUCTION CAM MECHANISMS

Mern Keat Lee

Department of Mechanical Engineering
McGill University, Montréal

April 2001

A Thesis submitted to the Faculty of Graduate Studies and Research
in partial fulfilment of the requirements for the degree of
Master of Engineering

0-612-70237-5

ABSTRACT

Cam mechanisms are widely used in industry, in applications requiring quick-return and indexing motions. A current research effort at the Robotic Mechanical Systems Laboratory of McGill University's Centre for Intelligent Machines aims at the application of cam mechanisms as speed reducers. The accuracy required in these mechanisms is of the utmost importance, especially when cams are rotating at a high speed.

In this thesis, the design for manufacturability of planar speed-reduction cam mechanisms is studied. In particular, the thesis focuses on a speed reducer with a rotating follower to couple shafts of parallel axes, termed planar Speed-o-Cam. Principles of the design for manufacturability are applied to Speed-o-Cam and a unified method for obtaining the optimum parameters satisfying the curvature constraints and pressure-angle bounds is developed. These two factors are relatively important because Numerically Controlled and Computer Numerically Controlled machine tools could be very sensitive to changes of curvature of the workpiece, especially when milling complex shapes such as those of cam plates.

Cam-mechanism balancing is also studied because unbalance in a high-speed rotating element can cause severe vibrations and greatly affect the bearings and hence, the performance of the machine. This is done by not only adding counterweights, which unavoidably increase the weight and volume of the mechanism, but also by removing material.

RÉSUMÉ

Les mécanismes à cames sont largement utilisés dans les applications nécessitant un mouvement de retour rapide et d'indexage. Un effort de recherche en cours au Laboratoire des systèmes mécanorobotiques du Centre pour les Machines Intelligentes de l'Université McGill a pour but l'utilisation de mécanismes à cames comme reducteurs de vitesse. La précision requise dans ces mécan'smes est de la plus grande importance, spécialement lorsque les cames tournent à une grande vitesse.

Dans cette thèse, la conception pour la fabrication de mécanismes planaires à cames fonctionnant comme réducteurs de vitesse est abordée. Spécialement, un réducteur de vitesse couplant des arbres à axes parallèles, appelé Speed-o-Cam planaire, est étudié. Les principes de conception pour la fabrication sont appliqués à Speed-o-Cam et une méthode unifiée pour obtenir les paramètres optimaux satisfaisant les contraintes de courbure et les bornes imposées sur l'angle de pression est dévelopée. Ces deux facteurs sont relativement importants parce que les machines-outils à commande numérique pourraient être très sensibles aux changements de courbure de la pièce, particulièrement lors de l'usinage des formes complexes comme celles des cames.

L'équilibrage du mécanisme à cames est aussi étudié puisque le déséquilibre d'un élément tournant à haute vitesse peut causer des vibrations importantes et grandement affecter les roulements et, en conséquence, la performance de la machine. Ceci, non seulement en ajoutant des contrepoids, qui invariablement augment le poids et la volume du mécanisme, mais aussi en enlevant du matériau.

ACKNOWLEDGEMENTS

I would like to thank my thesis supervisor *Professor Jorge Angeles*, for his support, encouragement and guidance in the work reported in this thesis. His profound knowledge in the area and his concern in high-quality research, played the most important role during the course of my work.

I would like to thank: Dr. Max A. González-Palacios for his clarification of many concepts in my research area; our industrial partners in the Speed-o-Cam project, Alta Precision and Placage Unique, for their assistance in producing the new Speed-o-Cam prototype; Ziontech Pte. Ltd., in Singapore, for providing valuable ideas and information, especially the manufacturing-error plots; and Pierre Montagnier, for helping me in translating the French version of the abstract.

I would also like to thank my collegues at Centre for Intelligent Machines (CIM) and of the Department of Mechanical Engineering, McGill University, for their help, support, useful comments, and making my stay at CIM a pleasant experience.

I am grateful to my parents and my whole family for their constant encouragement and support, which gave me confidence in completing my thesis. Last but not least, I would like to thank Say Hong Tan for not only sharing her love, but bearing with me by any means.

TABLE OF CONTENTS

ABSTRACT ii

RÉSUMÉ iii

ACKNOWLEDGEMENTS iv

LIST OF FIGURES vii

LIST OF TABLES x

CHAPTER 1. Introduction 1

1. Background 2

1.1. NC vs. CNC Machines Tools 4

2. Literature Review 5

3. Motivation 9

CHAPTER 2. Synthesis of the Planar Cam Mechanism 12

1. Geometry of Planar Cam Mechanism With Oscillating Roller-Followers 12

2. Geometry of the Cam Profile 14

3. Cam-Profile Determination 17

4. Cam-Curvature Determination 20

CHAPTER 3. The Influence of Profile Curvature on Manufacturability . . . 24

1. Machinability of the Cam Profile 24

2. Fourier Analysis of the Curvature of the Cam Profile 26

CHAPTER 4. Cam Synthesis 30
1. Curvature Constraints 30
2. Undercutting Avoidance 33
3. Pressure-Angle Constraints 35

CHAPTER 5. Dynamic Balancing of Planar Speed-o-Cam 39
1. Low-Speed Shaft 40
2. High-Speed Shaft 40
2.1. Material removal 41
2.2. Material addition 48

CHAPTER 6. Concluding Remarks 53
1. Conclusions 53
2. Recommendations for Future Research 54

REFERENCES 57

LIST OF FIGURES

1.1	Current Speed-o-Cam prototype: (a) overview; (b) detail view	3
1.2	General follower-displacement programs: (a) for DRDR; (b) for speed reduction	3
1.3	Types of cam follower mechanism : (a) planar; (b) spherical; (c) spatial (Courtesy of Sankyo America, Inc.)	6
1.4	Disk cams: (a) knife-edge follower; (b) roller follower; (c) flat-face follower	6
1.5	(a) Wedge cams; (b) spiral cam; (c) conjugate-cam mechanism	7
1.6	(a) Concave and (b) convex globoidal cams	7
1.7	(a) Cylindrical and (b) conical cams	7
1.8	Plot of cam profile with concavity	10
1.9	Error plot of the convex part of the cam (Courtesy of Ziontech Pte. Ltd., Singapore)	11
1.10	Error plot of the concave part of the cam (Courtesy of Ziontech Pte. Ltd., Singapore)	11
2.1	Layout of an oscillating roller-follower cam mechanism	13
2.2	Layout of an oscillating roller-follower cam mechanism	15
2.3	Planar Speed-o-Cam: (a)internal; (b) external (Courtesy of (González-Palacios and Angeles, 1993))	16

2.4 Layout of cam profile for planar Speed-o-Cam 18

2.5 Radius of curvature 22

2.6 Dimensionless curvature distribution of external Speed-o-Cam: (a) for $r = 0.8200$; (b) for $r = 0.7901$ 23

3.1 Spectrum for the dimensionless curvature of (a) the concave cam profile; (b) the convex cam profile 29

3.2 Phase plots for the dimensionless curvature of (a) the concave cam profile; (b) the convex cam profile 29

4.1 An example of a pseudo-convex cam, generated with the parameters, $N = 5$, $r = 0.88$ and $a_1 = 75$mm: (a) the pseudo-convex pitch curve; (b) its cam profile 33

4.2 Feasible convex cam profiles of external Speed-o-Cam: (a) for $N = 8$, with $r = 0.7901$ and $a_1 = 100$mm; (b) for $N = 5$, with $r = 0.6944$ and $a_1 = 75$mm 34

4.3 Feasible convex cam profiles of internal Speed-o-Cam: (a) for $N = 8$, with $r = 1.3061$ and $a_1 = 100$mm; (b) for $N = 5$, with $r = 1.5625$ and $a_1 = 100$mm 35

4.4 Pressure angle of an oscillating roller-follower cam mechanism . 36

4.5 Pressure-angle distribution for external Speed-o-Cam of two conjugate cams with parameters $r = 0.6944$ and $N = 5$ vs. ψ 37

5.1 Cam plate with three holes drilled 41

5.2 Cam plate designated for locus P 43

5.3 An example plot of d vs. R 45

5.4 An example of a cam plate with three holes bored 46

5.5 Camshaft created in Pro/Engineer: (a) side view; (b) perspective 46

5.6 Free-body diagram of camshaft 48

5.7 Diagram for moment balance 49

5.8 Circular counterweight proposed for planar Speed-o-Cam . . . 51

5.9 Camshaft with counterweights, created in Pro/Engineer: (a) side view; (b) perspective. 52

6.1 New design of external planar Speed-o-Cam with $N = 5$ (a) perspective view; (b) details view 54

6.2 Cam plates bored with (a) three holes; (b) one noncircular hole 55

LIST OF TABLES

4.1 Pressure angle of external Speed-o-Cam for various values of r with $N = 5$ 37

4.2 Pressure angle of external Speed-o-Cam for various values of r with $N = 8$ 38

4.3 Pressure angle of internal Speed-o-Cam for various values of r with $N = 8$ 38

CHAPTER 1

Introduction

A cam-follower mechanism is a mechanical device that transmits force or torque from cam to follower through a specific motion program by *higher-pair* contact. The nature of contact in a higher pair is along a line or at a point, while that in a lower pair is along a surface (Denavit and Hartenberg, 1964).

Common applications of cam mechanisms include quick-return and indexing motions. Quick-return mechanisms are extensively used in manufacturing processes such as metal-cutting, metal-forming, pick-and-place and material-handling operations. However, the applications of these mechanisms for speed reduction is still in its infancy.

The design of the foregoing transmissions relies on a unified methodology of indexing-cam-mechanism (ICM) design, which is based on the pure-rolling condition in the case of planar and spherical mechanisms; in the case of spatial mechanisms, the methodology is based on the minimum-sliding condition (González-Palacios and Angeles, 1993). With these features, the main drawbacks of gear transmissions, namely, backlash, high friction and high compliance, are expected to be eliminated.

The main thrust of the thesis is the design of speed-reduction cam mechanism for *manufacturability*. The term manufacturability began to be used in the 1960s to indicate the ease with which a part could be manufactured. It gradually became popular among those interested in the approach, and about 1985, *design for manufacturability* (DFM) came into wide use (Bralla, 1999).

Although the principles of DFM and its applications are not new, use of the term DFM and recognition of it as a sound design specification, within an organized design methodology, are recent.

The basic principles of DFM aim at a high-quality and cost-effective production. In order to manufacture parts at a minimum cost but with a high quality, a few considerations are taken into account: simplicity of the design; use of standard components; reduction of direct and indirect labour; use of general-purpose machine tools; reduction of manufacturing error; and use of *Computer Aided Design* (CAD)/*Computer Aided Manufacturing* (CAM) systems.

1. Background

Cam design is a synthesis process in which the required cam shape is determined to meet a prescribed set of displacement, velocity or accelaration conditions, sometimes as combinations thereof. The prescribed motion can be fully specified by a scalar function of a scalar variable, termed the *input-output function.*

The subject of this thesis is a specific type of planar speed-reducing cam mechanism, namely planar Speed-o-Cam, which is a speed reducer with a rotating follower to couple shafts of parallel axes. The research leading to this mechanism has been carried out at the Robotic Mechanical Systems Laboratory of McGill University's Centre for Intelligent Machines (CIM) for the past few years, the first prototype of planar Speed-o-Cam being shown in Fig. 1.1.

Figure 1.2(a) shows a general follower-displacement diagram, namely, of the dwell-rise-dwell-return (DRDR) type. In the case of Speed-o-Cam, the input-output function is prescribed as the linear function, shown in Fig. 1.2(b) (González-Palacios and Angeles, 1993).

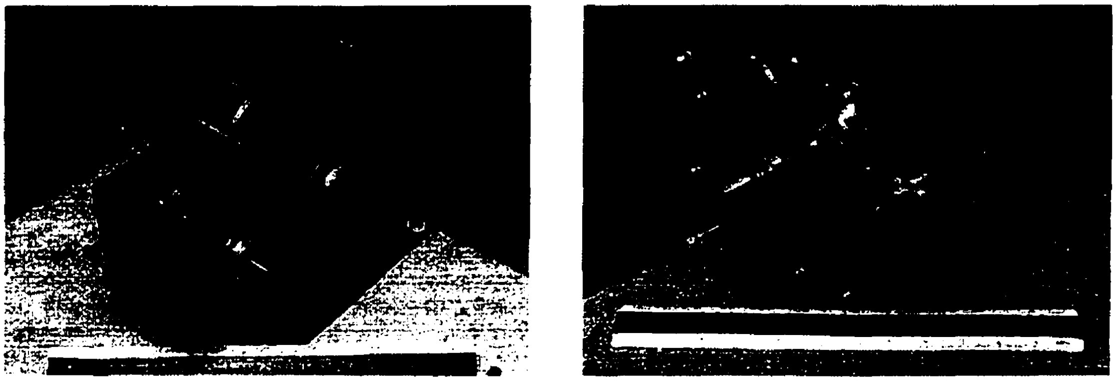

(a) (b)

FIGURE 1.1. Current Speed-o-Cam prototype: (a) overview; (b) detail view

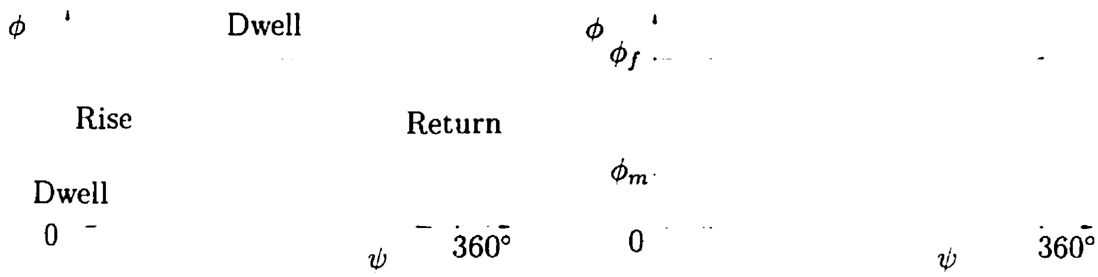

(a) (b)

FIGURE 1.2. General follower-displacement programs: (a) for DRDR; (b) for speed reduction

Cams have generally *complex* shapes, but the geometry of the cam plate is smooth *almost everywhere*. In the real-analytic sense, "almost everywhere" means "everywhere, except for a set of zero measure" (Taylor, 1985). Complex shapes in this context are defined as shapes that cannot be described with a simple formula; moreover, they are of a *non-analytic* type. In the general case, as shown in Fig. 1.2(a), the curve cannot be represented by a series expansion because of the constant slope during dwell. Therefore, in general, cam mechanisms entail an input-output function that is a non-analytic function of the input.

In order to produce complex-shape cam plates to high accuracy, sophisticated general-purpose *Computer Numerically Controlled* (CNC) machine tools are used. Factors that influence the performance of CNC machine tools are studied for manufacturability.

1.1. NC vs. CNC Machines Tools. Both *Numerically Controlled* (NC) and CNC machine tools are used to manufacture complex-shape workpieces. Nevertheless, there are some differences between the two types of machine tools. Loosely speaking, NC machine tools are older generations of CNC machine tools.

NC controls are also called hard-wired controls, which mean that their integrated-circuit digital packages are mounted and wired in a permanent arrangement, while CNC controls use a programmable computer with a read-write memory to control the machine tool. The control signals that NC and CNC systems receive are also different in that the former use voltage pulses, while the latter digital bits (Lin, 1994).

CNC systems, contrary to NC systems, have a storing memory, allowing part programs to be manually created or edited directly on the machine-tool control panel, besides having multi-tasking operations. The foregoing feature increases the productivity, while maximizing tool functionality (Besant, 1983). In addition, CNC machine tools are simpler to operate, more versatile, cheaper to maintain and more accurate to perform contouring operations than NC machine tools.

The usage of CNC machine tools has been enhanced by parallel advances in CAD/CAM. Integrated CAD/CAM systems use computers as a link between design and manufacturing. CNC machine tools, which are connected to CAD/CAM systems, are capable of producing complex three-dimensional surfaces to a high accuracy.

In cam manufacturing, CNC machine tools are used because of the advantages of CNC over NC machine tools. Higher accuracy, higher level of precision and consistency in machine computer control can be obtained with CNC machine tools, compared with those which are manually controlled. CAD/CAM systems provide data directly for the control of the manufacturing processes, thus bypassing the cost and lead time required for engineering drawings and process-programming.

2. Literature Review

Many classifications of cam mechanisms according to different criteria are available, e.g., (Angeles and López-Cajún, 1991) according to

- the relative layout of the axes of the cam and the follower
  - planar, in which the axes of motion of cam and follower are parallel to each other, as in Fig. 1.3(a).
  - spherical, in which all axes of relative motion are concurrent, as in Fig. 1.3(b).
  - spatial, in which the axes of motion of cam and follower are skew, as in Fig. 1.3(c).
- the input and output types of motion
  - translating, the cam or the follower undergoes pure translation.
  - rotating, the cam or the follower undergoes pure rotation.
- the physical shape of the follower
  - knife-dege, roller and flat-face follower, as shown in Fig. 1.4(a), (b) and (c), respectively.
- the physical shape of the cam
  - disk or plate cam, in which the axis of rotation of the cam is perpendicular to the plane of the follower motion, as in Fig. 1.4.
  - wedge cam, as shown in Fig. 1.5(a).
  - spiral cam, as shown in Fig. 1.5(b).
  - conjugate cams, whereby two cams are mounted rigidly on the same shaft and drive the same follower, as shown in Fig. 1.5(c).
  - globoidal cam, as shown in Fig. 1.6.
  - cylindrical and conical cams, as shown in Figs. 1.7(a) and (b), respectively.

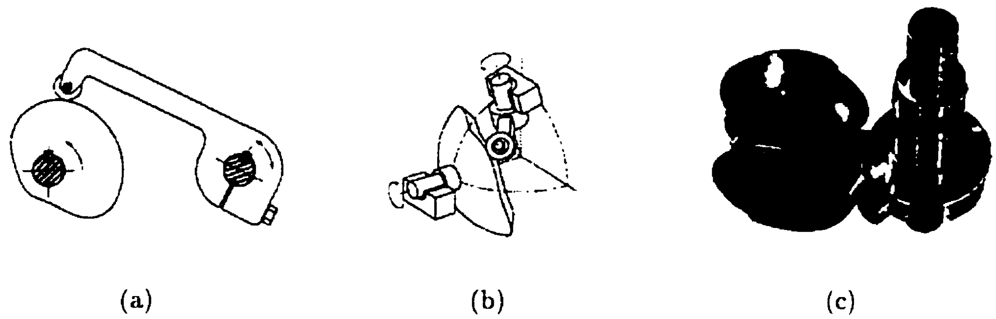

FIGURE 1.3. Types of cam follower mechanism : (a) planar; (b) spherical; (c) spatial (Courtesy of Sankyo America, Inc.)

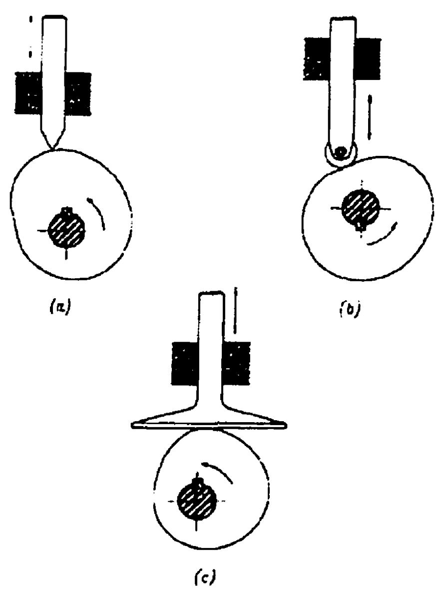

FIGURE 1.4. Disk cams: (a) knife-edge follower; (b) roller follower; (c) flat-face follower

An important factor affecting the performance of CNC machine tools is the curvature of the workpiece to be machined. Every NC and CNC machine tool has a finite bandwidth and can only respond to a certain range of working frequencies. In the presence of a sharp change in the curvature of the workpiece, a high demand on the frequency response of machine tools is required. Furthermore, chattering effects

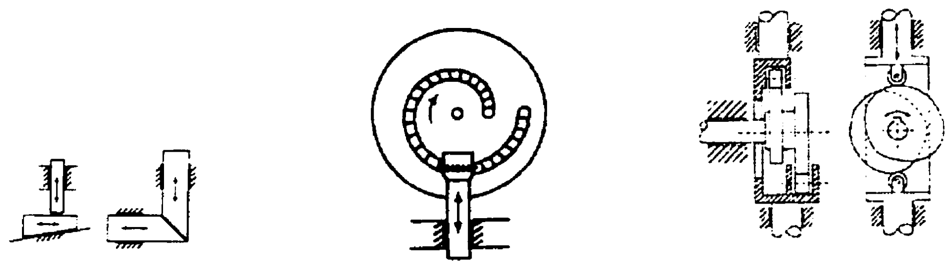

(a) (b) (c)

FIGURE 1.5. (a) Wedge cams; (b) spiral cam; (c) conjugate-cam mechanism

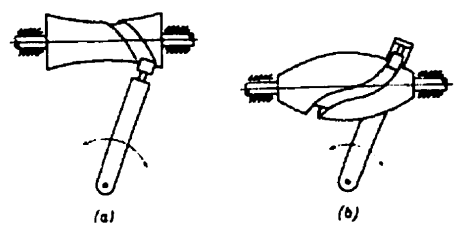

FIGURE 1.6. (a) Concave and (b) convex globoidal cams

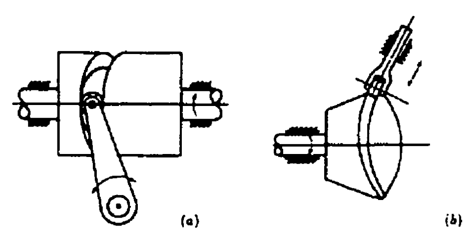

FIGURE 1.7. (a) Cylindrical and (b) conical cams

might become a severe matter if resonance occurs due to the high change in the curvature of the workpiece (Tobias, 1965; Welbourn and Smith, 1970). Hence, workpiece curvature, which in our case pertains to the cam profile, is a key issue that affects the accuracy of the machining and, thus, the performance and life span of the machine element under production (Rothbart, 1956).

Taguchi's concept of the *signal-to-noise* (S/N) ratio is famous in robust technology development (Taguchi, 2000; Wilde, 1991). In quality engineering, this concept has a wide range of applications, as it is used in evaluating the quality of a product or a manufacturing process. In this thesis, robust engineering is used as a guideline to derive a new concept, *machinability*, enhancing the cam manufacturability. Since machinability and Taguchi's S/N ratio are both defined, in their elementary forms, as ratios of mean to variance of a signal, our target is to minimize signal variability (Ross, 1996; Taguchi, 1988; Wu and Wu, 2000).

With regard to cam design, two phenomena, undercutting and cusp occurence, are additional matters of concern in the presence of roller followers. Undercutting occurs when the radius of the roller is greater than or equal to the minimum absolute value of the radius of curvature of the pitch curve, which is defined as the path generated by the centre of the follower as this moves around the cam. Cusps occur in cams when the tangent of the profile becomes undefined. These two phenomena should be avoided in cam designs (González-Palacios and Angeles, 1993; Norton, 1999).

The pressure angle is another function of merit in cam design. This is defined as the angle between the common normal at the cam-roller contact point and the velocity of the follower (Chen, 1982). The pressure angle plays an important role in cam design, although it is not directly related to DFM. The smaller the absolute value of the pressure angle, the better the force transmission (Hirschhorn, 1962). In the case of high-speed operations, i.e. angular velocities of cams exceeding 50 rpm, the recommended bounds of the pressure angle are within 30° (Malik, Ghosh and Dittrich, 1994; Navarro-Martínez, Wu and Angeles, 2001).

Rotor balancing is necceasry for rotating machinery, especially rotors operating under high speed. Due to the presence of eccentricity of the mass centre of a rotating machine element, centrifugal forces are generated when the shaft is in motion, the concurrent action of all these forces giving rise to what is known as gyroscopic moments. Consequently, the bearings will be subject to high dynamic loads, while the supporting shaft will deform significantly under the action of these unbalance forces (Darlow, 1989; Norton, 1999), and even enter in resonance.

3. Motivation

The performance and life expectancy of cam mechanisms are given due attention in this thesis. Technological developments in manufacturing methods, measurement technology, material selection and material treatments are among the main factors that influence the performance and life span of cam mechanisms, and, for that matter, of mechanical systems at large.

CNC machine tools provide high accuracy in milling complex shapes. But these sophisticated machines, as any physical system, exhibit their own limitations, especially with regard to their *speed of response*, characterized by their bandwidth. These limitations affect the accuracy with which these machines can cut profiles with high curvature changes.

Higher accuracy and better surface finish are obtained when a larger machine tool is chosen. If there exists a concavity in the workpiece, the machine tool is limited to a certain size when machining the concave section to avoid overcutting the convex part. Moreover, the effect of chatter arises when machining a workpiece with high curvature changes.

Some manufacturing problems were reported in the production of the first prototype of planar Speed-o-Cam. Error plots between the masterpiece and the actual workpiece manufactured by Ziontech Pte. Ltd., of Singapore, are shown in Figs. 1.9 and 1.10. In these figures, the horizontal axis represents the arc length along the cam profile and the vertical axis represents the manufacturing error. Figure 1.10 shows the error when manufacturing the concave part of the cam, i.e. section ABC in Fig. 1.8, while Fig. 1.9 shows the error when manufacturing the convex cam parts.

In Fig. 1.9, the vertical axis spans from -1.00μm to 1.00μm with equally divided intervals of 0.2μm, the horizontal axis indicating the arc length along the convex part of the cam machined; in Fig. 1.8, the vertical axis spans from -2.50μm to 2.50μm with equally divided intervals of 0.5μm, the horizontal axis indicating the arc length along the concave part of the cam machined.

From the error plots obtained, machining a convex shape of the cam induced a maximum error of 0.5μm, while machining a concave shape of the cam induced an error of up to 2.5μm. Obviously, this indicates a noticeably higher error, of 500%, in milling a concave cam. It is noteworthy that the cam profile, with identical geometry, machined by our local industrial partner, Ville d'Anjou's Alta Precision, exhibited a similar error distribution, although this was not quantified.

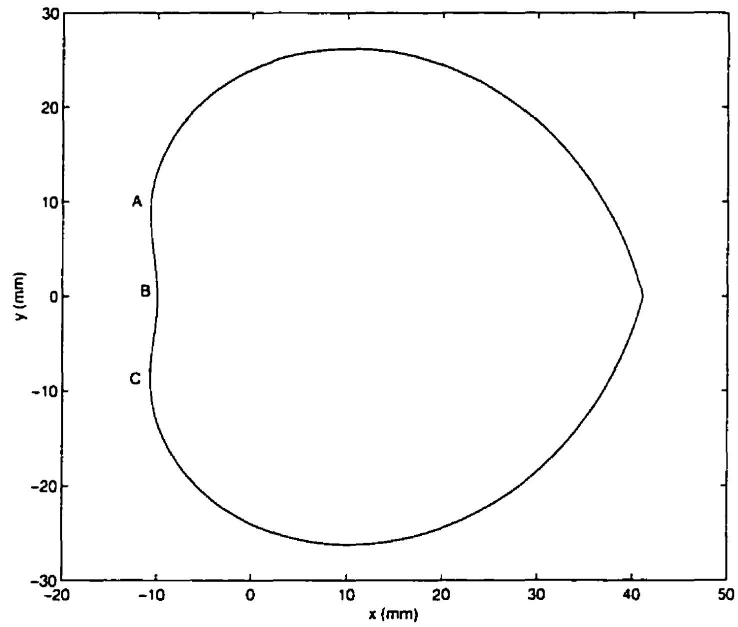

FIGURE 1.8. Plot of cam profile with concavity

The main contribution of this thesis is the study of the curvature constraints and pressure-angle distribution on cams, in order to minimize the manufacturing errors. Rotor balancing of planar Speed-o-Cam, aiming at minimizing the mass of the counterweights, is also given due attention.

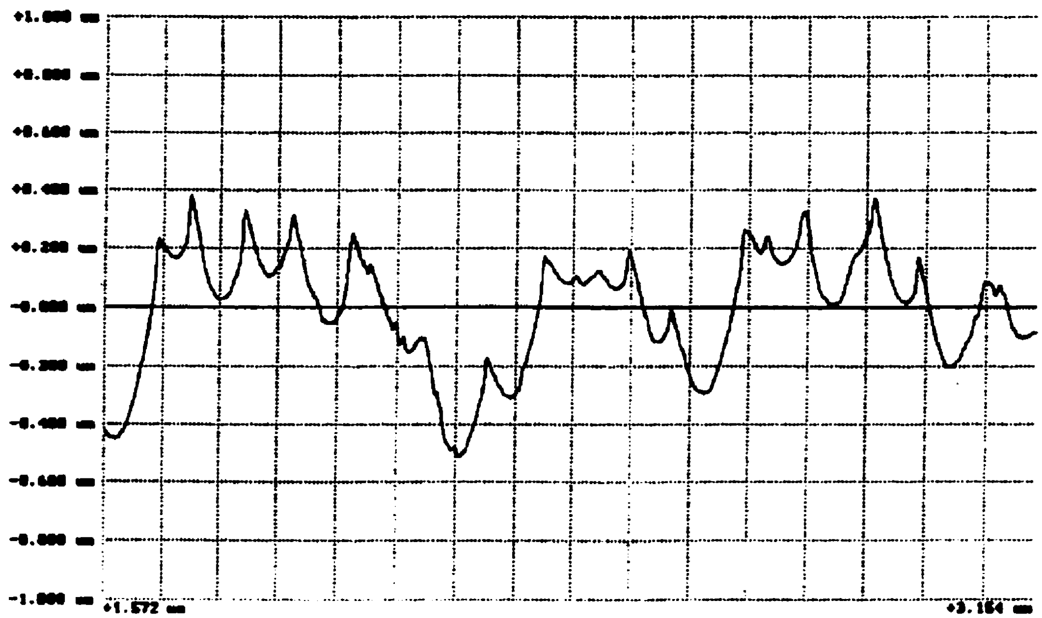

FIGURE 1.9. Error plot of the convex part of the cam (Courtesy of Ziontech Pte. Ltd., Singapore)

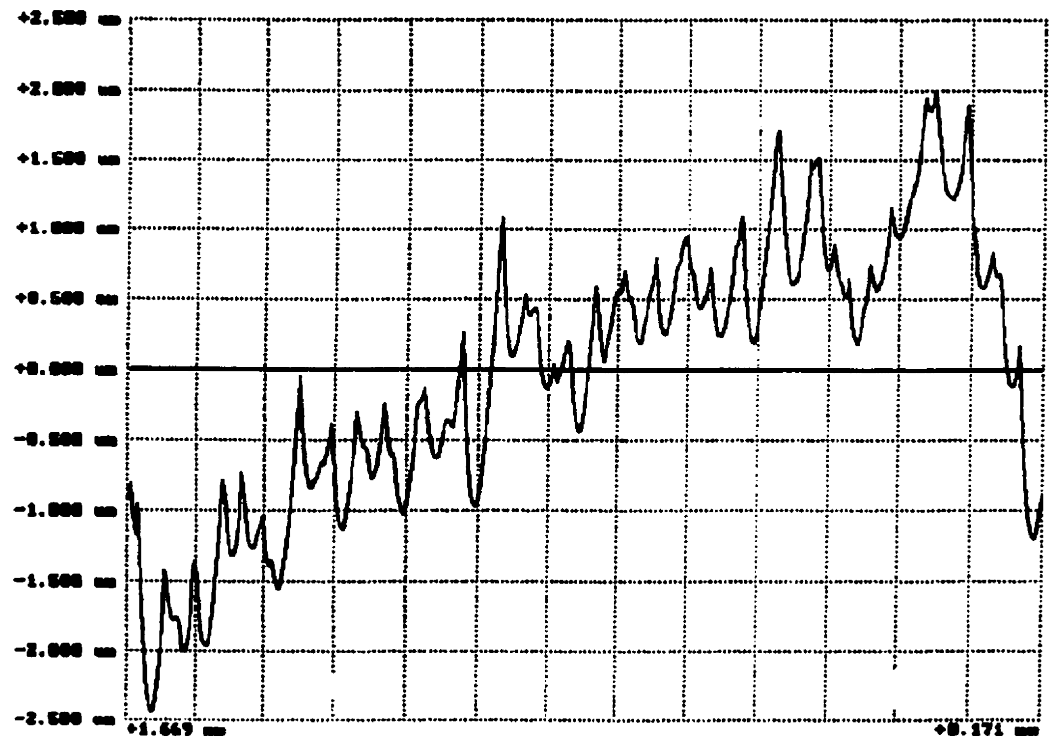

FIGURE 1.10. Error plot of the concave part of the cam (Courtesy of Ziontech Pte. Ltd., Singapore)

CHAPTER 2

Synthesis of the Planar Cam Mechanism

Generally speaking, cam mechanisms are composed of at least three elements: a cam, which is the driver; a follower, which is the driven element; and a fixed frame. The cam may remain stationary, translate, oscillate, or rotate, whereas the follower may tranlsate or oscillate. In some cases, a roller is included between cam and follower to reduce friction, contact stresses and wear.

In this chapter we will study the planar oscillating roller-follower cam mechanism. The first section describes the geometry of a general planar oscillating roller-follower cam mechanism. The sections thereafter discuss the geometry of the cam profile, determination of the cam-profile coordinates, and the curvature of the cam profile, designed specifically for a planar Speed-o-Cam, with a speed reduction of $5:1$ and its simplified morphology, as compared with the first prototype, as shown in Fig. 1.1.

1. Geometry of Planar Cam Mechanism With Oscillating Roller-Followers

The planar oscillating roller-follower cam mechanism, a planar four-link mechanism, comprises a cam that rotates about an axis, and a follower supplied with a roller, of radius a_4, rotating about the follower centre at a fixed distance a_3 from the follower centre. Moreover, a_1 is the fixed distance between the cam axis of rotation and the follower centre, as shown in Fig. 2.1. An ICM bears the morphology of the basic mechanism of Fig. 2.1, but with a multiplicity of equally-spaced rollers on its follower.

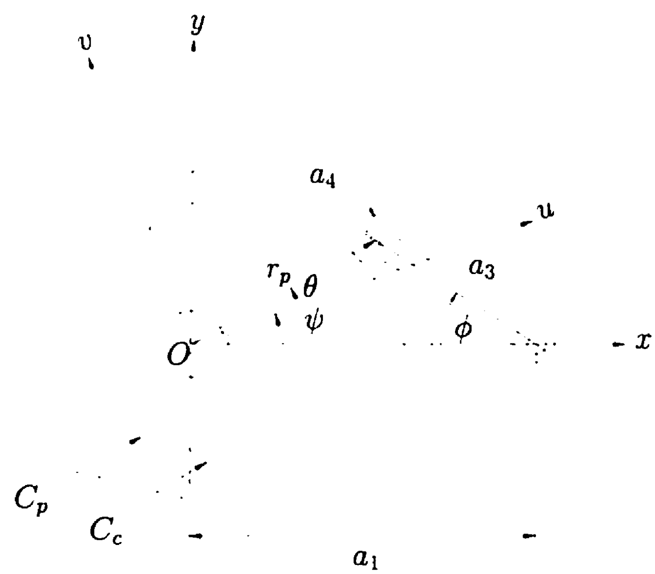

FIGURE 2.1. Layout of an oscillating roller-follower cam mechanism

In Fig. 2.1, frames u-v and x-y are attached to the cam and to the fixed frame, respectively. The notation used is described below:

C_c	:	cam profile;
C_p	:	pitch curve;
ψ	:	angular displacement of the cam;
ϕ	:	angular displacement of the follower;
r_p and θ	:	polar coordinates describing the pitch curve C_p in the u-v plane; $r_p = \sqrt{u_p^2 + v_p^2}\,; \theta = \arctan(v_p/u_p)$;
a_1	:	distance between the input and output axes;
a_3	:	distance between the output and roller axes;
a_4	:	radius of the roller.

In the above notation, which is adapted from that proposed by Denavit and Hartenberg (1964) for lower-pair mechanisms, no a_2 is present because of the special nature of cam mechanisms.

The Cartesian coordinates of the pitch curve in the u-v plane can be obtained from the geometry relations of Fig. 2.1 as

$$u_p(\psi) = a_1 \cos\psi - a_3 \cos(\psi + \phi) \tag{2.1}$$

$$v_p(\psi) = -a_1 \sin\psi + a_3 \sin(\psi + \phi) \tag{2.2}$$

González-Palacios and Angeles (1993) derived the cam profile coordinates for planar Speed-o-Cam, with the angular displacement $\tilde{\phi}$ of the follower used instead of ϕ, $\tilde{\phi}$ being defined as $\tilde{\phi} = \pi - \phi$, as shown in Fig. 2.2. We substitute this relation into eqs.(2.1) and (2.2) to be consistent of the notation for both pitch-curve and cam-profile coordinates throughout this thesis, thereby obtaining

$$u_p(\psi) = a_1 \cos\psi + a_3 \cos(\psi - \tilde{\phi}) \tag{2.3}$$

$$v_p(\psi) = -a_1 \sin\psi - a_3 \sin(\psi - \tilde{\phi}) \tag{2.4}$$

2. Geometry of the Cam Profile

Following the Aronhold-Kennedy Theorem (Veldkamp, 1976) and the concept of instantaneous screw axis, the Cartesian coordinates of the cam profile for planar Speed-o-Cam in the u-v plane are readily obtained as (González-Palacios and Angeles, 1993)

$$u_c(\psi) = b_2 \cos\psi + (b_3 - a_4)\cos(\psi - \delta) \tag{2.5}$$

$$v_c(\psi) = -b_2 \sin\psi - (b_3 - a_4)\sin(\psi - \delta) \tag{2.6}$$

where

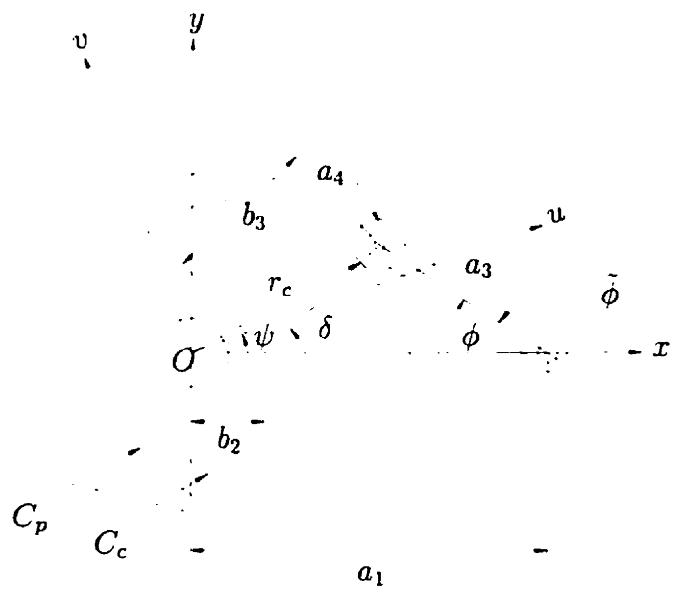

FIGURE 2.2. Layout of an oscillating roller-follower cam mechanism

$$b_2 = \frac{\bar{\phi}'}{\bar{\phi}' - 1} a_1 \tag{2.7}$$

$$b_3 = \sqrt{(a_3 \cos\bar{\phi} + a_1 - b_2)^2 + (a_3 \sin\bar{\phi})^2} \tag{2.8}$$

$$\delta = \arctan\left(\frac{a_3 \sin\bar{\phi}}{a_3 \cos\bar{\phi} + a_1 - b_2}\right) \tag{2.9}$$

with the notation described below:

ψ : angle of rotation of the cam:

$\bar{\phi}$: angular displacement of the follower;

$\bar{\phi}'$: derivative of the angular displacement of the follower with respect to ψ;

a_1 : distance between the input and output axes;

a_3 : distance between the output and roller axes;

a_4 : radius of the roller;

N : number of indexing steps, its reciprical being the speed-reduction ratio.

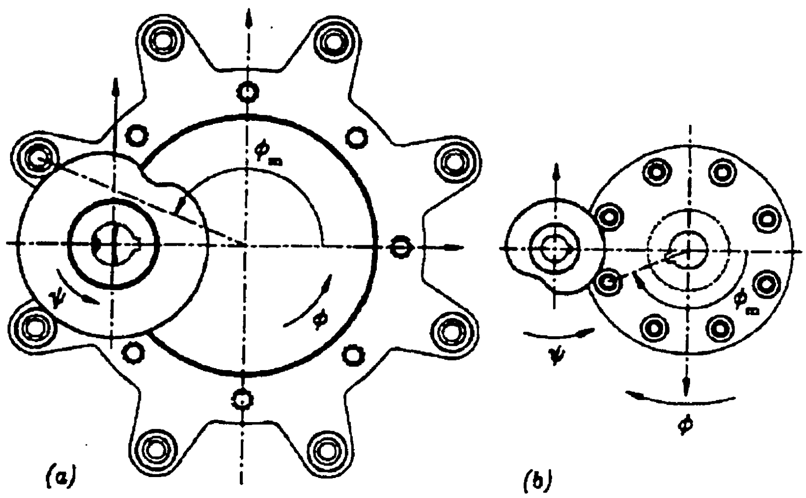

FIGURE 2.3. Planar Speed-o-Cam: (a)internal; (b) external (Courtesy of (González-Palacios and Angeles, 1993))

The input-output function of a general ICM is defined as (González-Palacios and Angeles, 1993)

$$\tilde{\phi} = \phi_m + \frac{2\pi}{N}\tau(x)\left(\frac{\psi}{\Delta\psi}\right) \tag{2.10}$$

where

- ϕ_m : the value of ϕ upon engagement of the roller with the cam, as shown in Fig. 2.3; $\phi_m = \pi(1 - 1/N)$;
- $\tau(x)$: a *normal* input-output function of the dimensionless variable x, for $0 \le x \le 1$ and $0 \le \tau(x) \le 1$.

For planar Speed-o-Cam, $\Delta\psi = 2\pi$ because the input and output functions entail a constant velocity for a full rotation of the cam, as in Fig. 1.2(b), and hence, $\tau(x) = x$ in our case.

In coupling shafts of parallel axes, two cases are distinguished, namely, internal and external layouts: in the former case, the input and output axes rotate in the same direction; in the latter case, the input and output axes rotate in the opposite direction, as shown in Fig. 2.3. Hence, for the internal layout of planar Speed-o-Cam, the input-output relationship takes the form

$$\tilde{\phi} = \pi\left(1 - \frac{1}{N}\right) + \frac{\psi}{N} \tag{2.11}$$

while the external Speed-o-Cam entails an input-output relationship of the form

$$\tilde{\phi} = -\left[\pi\left(1 - \frac{1}{N}\right) + \frac{\psi}{N}\right] \tag{2.12}$$

3. Cam-Profile Determination

Figure 2.4 shows the cam profile to be produced, with r_c and $\tilde{\theta}$ denoting the polar coordinates describing the cam profile, where $r_c = \sqrt{u_c^2 + v_c^2}$ and $\tilde{\theta} = \arctan(v_c/u_c)$. Segment $\overline{OP}$ is attached to the fixed frame, points A and B indicating the coordinates of the profile when $\psi = 0$ and 2π, respectively.

The Cartesian coordinates of the cam profile are needed in order to create a spline curve in CAD software, then integrating it into the CNC machine-tool code. Although we already have the Cartesian coordinates of the cam profile at hand, we need to obtain the interval of ψ to produce a fully-closed cam profile. This interval is determined by angles Δ, as shown in Fig. 2.4.

Using eqs.(2.5) and (2.6), and realizing that the u-axis is the axis of symmetry of the cam profile from Fig. 2.4, we can obtain Δ by setting

$$v_c(-\Delta) = 0 \tag{2.13}$$

$$v_c(\Delta + 2\pi) = 0 \tag{2.14}$$

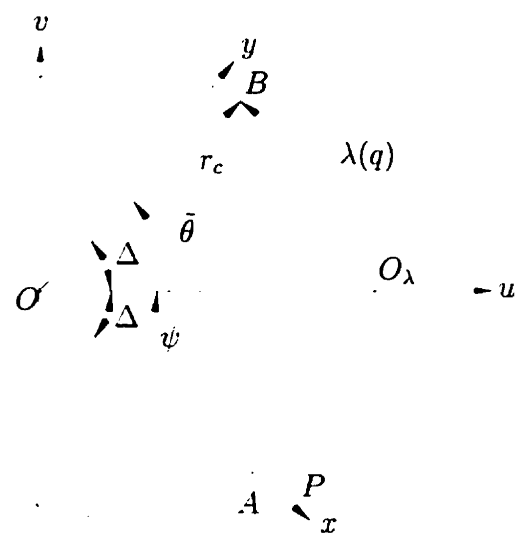

FIGURE 2.4. Layout of cam profile for planar Speed-o-Cam

In fact, both eqs.(2.13) and (2.14) will yield the same result, by virtue of the symmetry of the cam profile. Taking eq.(2.14), for example, we obtain

$$v_c(\Delta + 2\pi) \equiv -b_2 \sin(\Delta + 2\pi) - (b_3 - a_4)\sin(\Delta + 2\pi - \delta) = 0$$

which, upon expansion, reduces to

$$f(\Delta) \equiv -\frac{v_c(\Delta + 2\pi)}{b_2} = \sin\Delta + (b_3/b_2 - a_4/b_2)\sin(\Delta - \delta) = 0 \qquad (2.15)$$

with b_2, b_3 and δ introduced in eqs.(2.7)-(2.9). Note that eq.(2.15) is transcendental. Indeed, b_3 and δ are functions of $\bar{\phi}$, and $\bar{\phi}$ is a function of ψ, given by either eq.(2.11) or eq.(2.12), depending on whether the layout at hand is internal or, correspondingly, external. Because of the form of the foregoing functional relations, $f(\Delta)$ cannot be transformed into polynomial form. As a result, $f(\Delta)$ admits infinitely many solutions. To find one of these roots, we resort to the Newton-Raphson method (Hamming, 1962).

The roots of $f(\Delta)$ are thus found using the iterative scheme

$$\Delta_i = \Delta_{i-1} - \frac{f(\Delta_i)}{f'(\Delta_i)}$$

where $f'(\Delta)$ is the derivative of $f(\Delta)$ with respect to Δ. This procedure stops when $|\Delta_i - \Delta_{i-1}| \leq \epsilon$, for a prescribed tolerance ϵ.

Note that b_2 and a_4 are constants in $f(\Delta)$, whence $f(\Delta)$ can be written as $f(\Delta) = f(\Delta; b_3(\phi(\Delta)), \delta(\tilde{\phi}(\Delta))$ where $\tilde{\phi}(\Delta) = \pm[\pi(1 - 1/N) + \Delta/N]$, and $f'(\Delta)$ can be calculated using the chain rule:

$$f'(\Delta) = \frac{df}{d\Delta} = \frac{\partial f}{\partial \Delta} + \frac{\partial f}{\partial b_3}\frac{\partial b_3}{\partial \tilde{\phi}}\frac{d\tilde{\phi}}{d\Delta} + \frac{\partial f}{\partial \delta}\frac{\partial \delta}{\partial \tilde{\phi}}\frac{d\tilde{\phi}}{d\Delta}$$

where

$$\begin{aligned}
\frac{\partial f}{\partial b_3} &= \frac{\sin(\Delta - \delta)}{b_2} \\
\frac{\partial b_3}{\partial \tilde{\phi}} &= \frac{a_3}{b_3}(b_2 - a_1)\sin\tilde{\phi} \\
\frac{\partial f}{\partial \delta} &= -\left(\frac{b_3}{b_2} - \frac{a_4}{b_2}\right)\cos(\Delta - \delta) \\
\frac{\partial \delta}{\partial \tilde{\phi}} &= \frac{a_3}{b_3^2}(a_3 + a_1 - b_2) \\
\frac{d\tilde{\phi}}{d\Delta} &= \pm\frac{1}{N}
\end{aligned}$$

The positive sign of the doubly-signed terms in this section yields a cam for the internal planar Speed-o-Cam, whereas the negative sign a cam for its external counterpart. In any case, using $\psi_{min} = -\Delta$ and $\psi_{max} = 2\pi + \Delta$, a complete closed cam profile is readily computed using eqs.(2.5) and (2.6), together with eqs.(2.7)-(2.9), with parameter ψ varying in the interval

$$\psi_{min} \leq \psi \leq \psi_{max}$$

4. Cam-Curvature Determination

In general, for any parametric curve described by $\mathbf{p}(q)$, the curvature. κ of the curve can be found using the expression (Angeles and López-Cajún, 1991)

$$\kappa = \mathrm{sgn}[\lambda'(q)]\frac{\mathbf{p}''^{T}(q)\mathbf{E}\mathbf{p}'(q)}{||\mathbf{p}'(q)||^3} \tag{2.16}$$

For a planar profile, $\mathbf{p}(q) = x(q)\mathbf{i} + y(q)\mathbf{j}$, where $\mathbf{p}$ is the position vector of an arbitrary point on the curve parametrized with *any* parameter q; $\mathbf{i}$ and $\mathbf{j}$ denote the constant unit vectors in the x and y directions, respectively; $\lambda(q)$ measures the arc length of the curve from a reference point O_λ with q defined as in Fig. 2.4; $\mathrm{sgn}(\cdot)$ is the *signum* function of $(\cdot)$, which is defined as $+1$ if its argument is postive, -1 if its argument is negative, and 0 if its argument vanishes; $\mathbf{E}$ is a 2×2 orthogonal, skew-symmetric matrix, given as

$$\mathbf{E} = \begin{bmatrix} 0 & -1 \\ 1 & 0 \end{bmatrix}$$

It is natural to choose $q = \psi$ in this case, whence, apparently, $\lambda'(q) < 0$ if $q = \psi$, as shown in Fig. 2.4. Hence, $\mathrm{sgn}[\lambda'(\psi)] < 0$ and eq.(2.16) can be written in terms of $u(\psi)$ and $v(\psi)$ as

$$\kappa = \frac{v'(\psi)u''(\psi) - u'(\psi)v''(\psi)}{[(u'(\psi))^2 + (v'(\psi))^2]^{3/2}} \tag{2.17}$$

The sign of κ in eq.(2.17) tells whether the curve is convex or concave at a point: a positive κ implies a convexity while a negative κ implies a concavity at that point.

To obtain the curvature of the cam profile for a given roller follower, we make use of the Cartesian coordinates of the pitch curve, since the cam-profile Cartesian coordinates are too cumbersome for the purpose at hand, i.e., obtaining the first and second derivatives of the pitch curve is an easier task compared to that associated with the cam profile. Then, we obtain the curvature of the cam profile by a simple geometric relationship between the curvatures of the pitch curve and the cam profile.

From eqs.(2.3) and (2.4), the first and second derivatives of the pitch curve, with respect to the angle of rotation of the cam, ψ, can be readily obtained as

$$\begin{aligned} u_p'(\psi) &= -a_1 \sin(\psi) - a_3(1-\tilde{\phi}')\sin(\psi-\tilde{\phi}) && (2.18)\\ v_p'(\psi) &= -a_1 \cos(\psi) - a_3(1-\tilde{\phi}')\cos(\psi-\tilde{\phi}) && (2.19)\\ u_p''(\psi) &= -a_1 \cos\psi - a_3(1-\tilde{\phi}')^2\cos(\psi-\tilde{\phi}) + a_3\sin(\psi-\tilde{\phi})\tilde{\phi}'' && (2.20)\\ v_p''(\psi) &= a_1 \sin\psi + a_3(1-\tilde{\phi}')^2\sin(\psi-\tilde{\phi}) + a_3\cos(\psi-\tilde{\phi})\tilde{\phi}'' && (2.21) \end{aligned}$$

Now we introduce the non-dimensional parameter r, defined as

$$r = \frac{a_3}{a_1}$$

By substituing r along with eqs.(2.18), (2.19), (2.20), and (2.21) into eq.(2.17), the curvature, κ_p of the pitch curve can be obtained as

$$\kappa_p = \frac{1}{a_1}\frac{r^2(1-\tilde{\phi}')^3 + r[(1-\tilde{\phi}')(2-\tilde{\phi}')\cos\tilde{\phi} + \tilde{\phi}''\sin\tilde{\phi}] + 1}{[r^2(1-\tilde{\phi}')^2 + 2r(1-\tilde{\phi}')\cos\tilde{\phi} + 1]^{3/2}} \qquad (2.22)$$

Let ρ_c and ρ_p be the radius of curvature of the cam profile and the pitch curve, respectively. Since the curvature is the reciprocal of the radius of curvature, we have

$$\rho_c = \frac{1}{\kappa_c} \quad , \quad \rho_p = \frac{1}{\kappa_p}$$

From Fig. 2.5, it is apparent that

$$\rho_p = \rho_c + a_4 \qquad (2.23)$$

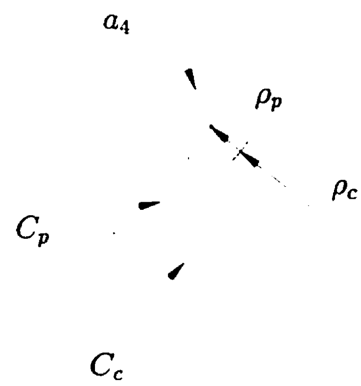

FIGURE 2.5. Radius of curvature

Writing eq.(2.23) in terms of κ_c and κ_p, we obtain the curvature of the cam profile as

$$\kappa_c = \frac{\kappa_p}{1 - a_4 \kappa_p} \tag{2.24}$$

with κ_p given in eq.(2.22).

Figures 2.6(a) and (b) show the curvature distribution for two different values of r, where $r = 0.8200$ corresponds to our current concave cam profile; $r = 0.7901$ corresponds to a fully convex cam profile with a minimum absolute value of curvature equal to zero. Notice that these figures show plots of the non-dimensional curvature, $a_1\kappa_c$ vs. angle ψ, where a_1 is taken as 100mm with a speed reduction of $8 : 1$. Figure 2.6(a) has a peak-to-peak value of 10.8990, while Fig. 2.6(b) has a peak-to-peak value of 5.2156.

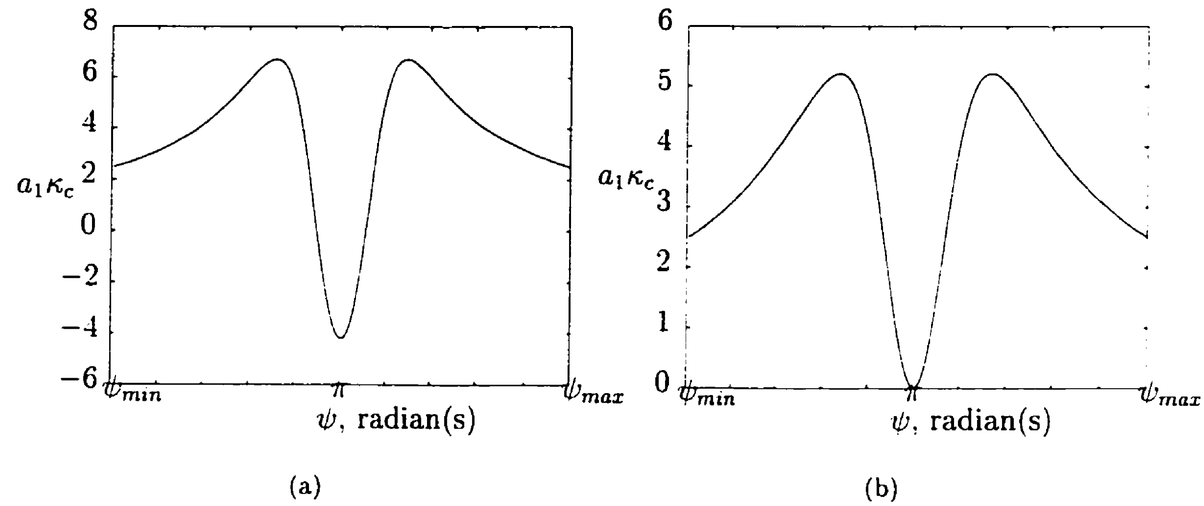

FIGURE 2.6. Dimensionless curvature distribution of external Speed-o-Cam: (a) for $r = 0.8200$; (b) for $r = 0.7901$

CHAPTER 3

The Influence of Profile Curvature on Manufacturability

One of the DFM principles is to produce high quality parts or, as pertaining to our case, to produce parts with the highest accuracy possible. In a cam mechanism, the accuracy of the cam profile is of the utmost importance because it is the most complicated part to machine. Moreover, a device with conjugate cam elements, like Speed-o-Cam, is geometrically overconstrained. In consequence, machining errors could lead to interference and hence, to lack of assemblability. A higher accuracy of a cam will also ensure a higher quality of force transmission and a longer life span of the mechanism.

In this chapter, the impact of the curvature of the cam profile on profile manufacturability is studied. A new concept in line with Taguchi's formulation of robust engineering is introduced to study the manufacturability of various curvature distributions of the cam profile. Fourier analysis is carried out to study the frequency content of the cam profile due to curvature changes in the workpiece.

1. Machinability of the Cam Profile

Intuitively, a circle is the most robust curve for a machine tool to follow, as it involves only one parameter to control, namely, its radius. Since there will be always environmental design parameters, which are beyond human control, a deviation from the nominal path will unavoidably occur, as a machine tool follows an arbitrary path.

To study the robustness of an arbitrary curve to machining errors, we introduce a measure called *machinability* to indicate how "close" a contour is from a circle, regardless of the scale involved.

In order to measure the deviation of an arbitrary curve to a circle, *loss of circularity* L is defined as the absolute value of the standard deviation σ of the curvature of the curve divided by the curvature mean value, $\bar{\kappa}$, i.e.,

$$L = \left|\frac{\sigma}{\bar{\kappa}}\right| \tag{3.1}$$

A zero L indicates no deviation, and, hence no loss of circularity, while an infinitely-large L denotes white noise in the curvature of the curve. To avoid dealing with infinitely-large values, machinability is then defined as

$$M = e^{-L} \times 100\% \tag{3.2}$$

where M measures the machinability of the curve, a percentage that lies between zero and 100: A value of $M = 0\%$ indicates white noise in the curvature of the curve; A value of $M = 100\%$ indicates the most robust contour with regard to machinability, namely, a circle.

Briefly speaking, a lower variability, i.e. a higher machinability, indicates a more robust design, which is consistent with the S/N ratio formulated by Taguchi. Therefore, the manufacturing error of a machine tool when cutting a contour decreases as the machinability increases.

Since our interest is in cam manufacturing, we focus on the curvature of the cam profile. In comparison with the machinability of the current concave cam design, reported in (González-Palacios and Angeles, 1999), and a fully convex cam, we use

$r = 0.7901$ (convex cam) and $r = 0.8200$ (current cam) for $N = 8$ and an external planar Speed-o-Cam as an example to illustrate the machinability index.

To obtain the mean $\bar{\kappa}_c$ and the unbiased standard deviation s of the curvature of the cam profile, we use (Bajpai, Mustoe and Walker, 1989)

$$\bar{\kappa}_c = \frac{1}{n}\sum_{i=1}^{n} \kappa_c(\psi_i) \quad (3.3)$$

$$s = \sqrt{\frac{1}{n-1}\sum_{i=1}^{n}[\kappa_c(\psi_i) - \bar{\kappa}_c]^2} \quad (3.4)$$

where n is the number of points on the cam profile and $\kappa_c(\psi_i)$ is the curvature value of the cam profile of $\psi = \psi_i$ at ith point.

The results show that $L_{\text{concave}} = 1.9965$ and $L_{\text{convex}} = 0.3125$. Hence, $M_{\text{concave}} = 13.58\%$ and $M_{\text{convex}} = 73.16\%$. Obviously, the convex cam design is about 5.4 times more robust than the current concave cam design. Hence, a fully convex cam should lead to lower manufacturing errors.

2. Fourier Analysis of the Curvature of the Cam Profile

Fourier's representation of a periodic function as a superposition of harmonic functions has a wide field of applications, including wavelet analysis, communication theory and signal analysis, which involves the study of noise in a signal (James, 1995).

In this section, Fourier analysis is applied to study a curvature signal to support the machinability concept introduced in Section 3.1. Fourier analysis works by first translating a time-domain, or space-domain signal into a frequency-domain signal. The signal can then be analyzed for its frequency content because the Fourier coefficients of the transformed signal represent the contribution of each harmonic component at each frequency. The frequency content is the most determinant factor of the quality of a signal, thus this section is motivated by the need to study the signal, or the frequency content of the contour at hand.

It follows from the Gibbs effect in Fourier analysis that any sound with a sharp pulse will have a rich high-frequency content; hence, a similar behaviour is expected in physical mechanical systems.

In Section 2.4, we show that a concave profile has a higher change in curvature with a peak-to-peak value of 10.8990, as opposed to the convex profile, which has a peak-to-peak value of 5.2156. Hence, a concave profile is expected to have a rich high-frequency in its spectrum, as compared to a convex profile.

We expect that low curvature changes in a profile will give a lower amplitude of the *fundamental frequency*, i.e. a lower amplitude of the lowest frequency, than in a profile with high curvature changes. We also expect a richer spectrum to be found in the profile with high curvature changes, and hence, to be manufacturable with lower accuracy.

The analysis is carried out specifically on the cam profile; however, this analysis applies to any profile without loss of generality.

We expect that there will be a difference in the spectrum between a cam with a convex profile and a cam with a concave profile. In the fully-convex cam case (low curvature changes), the amplitude of the fundamental frequency is expected to have a lower value than that of a contour with a concave cam case (high curvature changes). Moreover, the percentage reduction of the amplitude should be substantial in the fully-convex cam case.

The above analysis is conducted in order to explain the error plots reported by Ziontech Pte. Ltd., as shown in Figs. 1.9 and 1.10, because machining a workpiece with high curvature changes requires the CNC machine used to react beyond its capabilities: The machine tool, which has a finite bandwidth of working frequencies, might not respond fast enough under high changes of curvature in the workpiece. Moreover, a high percentage reduction of the amplitude ensures the machine tool to reach a stable operation in a shorter period, thereby reducing the likelihood of resonance occurence.

Fourier analysis has been applied to the curvature of the cam profile, with parameterization of $\kappa_c = \kappa_c(\psi)$, and the spectrum plots are compared between a convex cam profile and the current concave cam profile.

According to Fourier analysis (Bajpai, Mustoe, Walker, 1989), a periodic signal $f(x)$ can be expressed in the form

$$f(x) = a_o + \sum_{k=1}^{\infty}[a_k \cos(k\omega_o x) + b_k \sin(k\omega_o x)] = a_o + \sum_{k=1}^{\infty} c_k \cos(k\omega_o x + \phi_k)$$

where

$$\begin{aligned}
a_o &= \frac{\omega}{2\pi}\int_0^{2\pi/\omega_o} f(x)\,dx \\
a_k &= \frac{\omega}{\pi}\int_0^{2\pi/\omega} f(x)\cos(k\omega_o x)\,dx \qquad k = 1, 2, \cdots \\
b_k &= \frac{\omega}{\pi}\int_0^{2\pi/\omega} f(x)\sin(k\omega_o x)\,dx \qquad k = 1, 2, \cdots \\
c_k &= \sqrt{a_k^2 + b_k^2} \qquad k = 1, 2, \cdots \\
\phi_k &= -\arctan(b_k/a_k) \qquad k = 1, 2, \cdots
\end{aligned}$$

Figures 3.1 and 3.2 show the results of the magnitude and phase plots, respectively, after performing a Fourier analysis on the dimensionless curvature of the cam profile $a_1\kappa_c$, which is derived in Chapter 4.

When comparing Figs. 3.2(a) and (b), we do not see a perceptible difference in the phase distribution of the two profiles. However, when we compare Figs. 3.1(a) and (b), we notice that the amplitude of the fundamental frequencies of the concave plate is about twice as large as that of its convex counterpart. What this means is that the machine tool structure will be excited, upon tracing the concave cam profile, by a forcing signal that is about twice as large as that produced when tracing the convex profile.

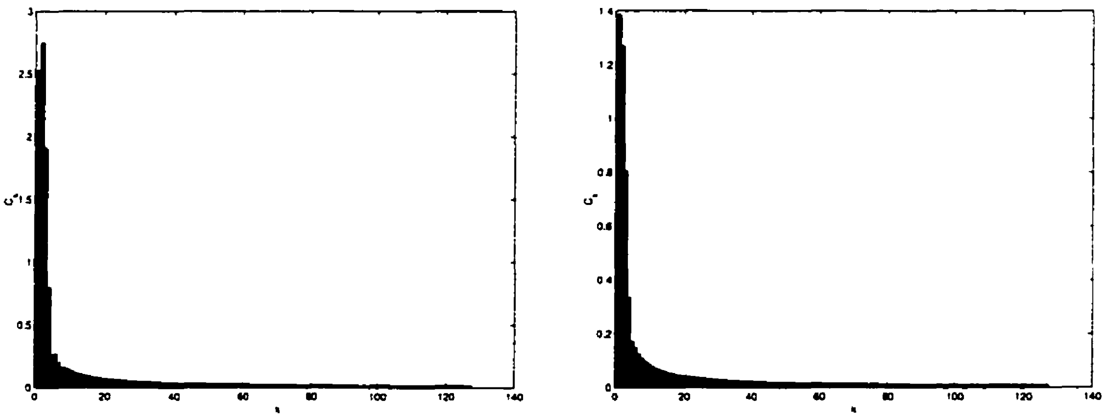

(a) (b)

FIGURE 3.1. Spectrum for the dimensionless curvature of (a) the concave cam profile; (b) the convex cam profile

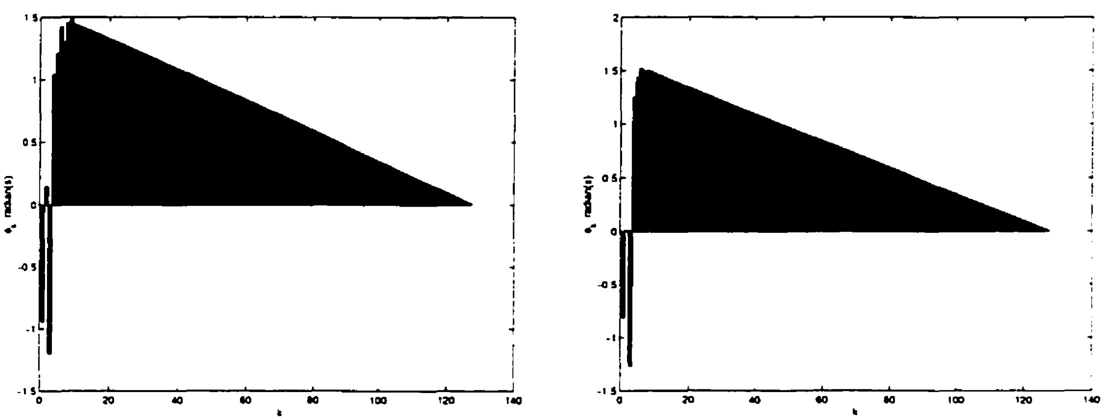

(a) (b)

FIGURE 3.2. Phase plots for the dimensionless curvature of (a) the concave cam profile; (b) the convex cam profile

Therefore, the Fourier analysis shows that a fully-convex workpiece is manufacturable with higher accuracy due to less forcing signal being excited to the machine tool structure, which apparently leads to an improvement in machinability.

CHAPTER 4

Cam Synthesis

In Chapter 3, we showed that cam-profile convexity is imperative for DFM purposes. This chapter proposes a systematic procedure which allows us to obtain fully-convex cam profiles in planar Speed-o-Cam and obey the maximum pressure angle bounds. First, the range of the parameters in which cam convexity is preserved is obtained. Then, parameter values which give the smallest maximum pressure angle of the mechanism are selected.

1. Curvature Constraints

Since we are interested in obtaining a fully-convex cam, we want to impose a condition on r guaranteeing that κ_c remains positive. The relationship between cam-profile and pitch-curve curvatures, κ_c and κ_p, respectively, leads to $1 - a_4\kappa_p > 0$ to be satisfied to avoid undercutting in roller-follower cam mechanisms (Wilson and Sadler, 1993). Hence, assuming that undercutting is avoided, from eq.(2.24), it is obvious that κ_c remains positive if and only if κ_p does.

If we multiply both sides of eq.(2.22) by a_1, we obtain a non-dimensional expression for the pitch-curve curvature, namely,

$$a_1\kappa_p = \frac{r^2(1-\tilde{\phi}')^3 + r[(1-\tilde{\phi}')(2-\tilde{\phi}')\cos\tilde{\phi} + \tilde{\phi}''\sin\tilde{\phi}] + 1}{[r^2(1-\tilde{\phi}')^2 + 2r(1-\tilde{\phi}')\cos\tilde{\phi} + 1]^{3/2}} \tag{4.1}$$

Let $f_1(r)$ and $f_2(r)$ be the numerator and denominator of eq.(4.1), respectively, i.e.,

$$f_1(r) = r^2(1-\tilde{\phi}')^3 + r[(1-\tilde{\phi}')(2-\tilde{\phi}')\cos\tilde{\phi} + \tilde{\phi}''\sin\tilde{\phi}] + 1 \tag{4.2}$$

$$f_2(r) = [r^2(1-\tilde{\phi}')^2 + 2r(1-\tilde{\phi}')\cos\tilde{\phi} + 1]^{3/2} \tag{4.3}$$

Further, let us recall that $f_2(r)$ is defined as $a_1\|\mathbf{p}'(q)\|^3$, and hence, it is always positive, the sign of $a_1\kappa_p$ thus depending solely on the sign of $f_1(r)$. Hence, convexity of the profile is preserved if and only if the condition below holds:

$$r^2(1-\tilde{\phi}')^3 + r[(1-\tilde{\phi}')(2-\tilde{\phi}')\cos\tilde{\phi} + \tilde{\phi}''\sin\tilde{\phi}] + 1 > 0 \tag{4.4}$$

By virtue of the linear relation between $\tilde{\phi}$ and ψ, $\tilde{\phi}' = \pm 1/N$, i.e. $\tilde{\phi}'$ is a constant, while $\tilde{\phi}'' = 0$, the positive sign being used for internal layouts and the negative sign for their external counterparts in planar Speed-o-Cam. For external layouts, eq.(4.4) becomes

$$r^2\left(1+\frac{1}{N}\right)^3 + r\left(1+\frac{1}{N}\right)\left(2+\frac{1}{N}\right)\cos\tilde{\phi} + 1 > 0$$

Now we study under which conditions the left-hand side of the above relation vanishes, which we try to avoid. Thus, we set the above left-hand side equal to zero and solve for $\cos\tilde{\phi}$ from the expression thus resulting, i.e.,

$$\cos\tilde{\phi} = -\frac{r^2(1+1/N)^3+1}{r(1+1/N)(2+1/N)} \tag{4.5}$$

For internal layouts, the same relation holds, except for the sign of $1/N$, which would be reversed. Hence, it is obvious that for the case of planar Speed-o-Cam, we have a κ_p that is always positive if the fraction of eq.(4.5) yields a complex value of $\tilde{\phi}$, i.e., if

$$\frac{r^2(1+1/N)^3+1}{r(1+1/N)(2+1/N)} > 1$$

or

$$\left(1+\frac{1}{N}\right)^3 r^2 - \left(1+\frac{1}{N}\right)\left(2+\frac{1}{N}\right) r + 1 > 0 \tag{4.6}$$

Inequality(4.6) holds for two ranges of r values, namely,

$$r > \frac{1}{1+1/N} \quad \text{and} \quad r < \frac{1}{(1+1/N)^2} \tag{4.7}$$

Hence, the intervals of eq.(4.7) give the condition on r for generating a fully-convex cam profile in the external layout. Similarly, one can show that the corresponding conditions on r for internal layouts are

$$r < \frac{1}{1-1/N} \quad \text{and} \quad r > \frac{1}{(1-1/N)^2} \tag{4.8}$$

The ranges of values of r that satisfy intervals (4.7) and (4.8) give a fully-convex cam profile in the external and the internal planar Speed-o-Cam, respectively. However, these conditions are neccesary, but not sufficient in describing a fully-convex cam. In fact, cases exist observing the foregoing constraints that lead to unacceptable cam profiles, which we term *pseudo-convex* profiles. An example illustrating this phenomenon is shown in Fig. 4.1 with $N = 5$, $r = 0.88$ and $a_1 = 75$mm, which satisfies the first interval (4.7) but does not yield a feasible cam profile. Necessary and sufficient conditions on r that guarantee a fully-convex, feasible cam profile are derived below upon imposing the condition to avoid undercutting.

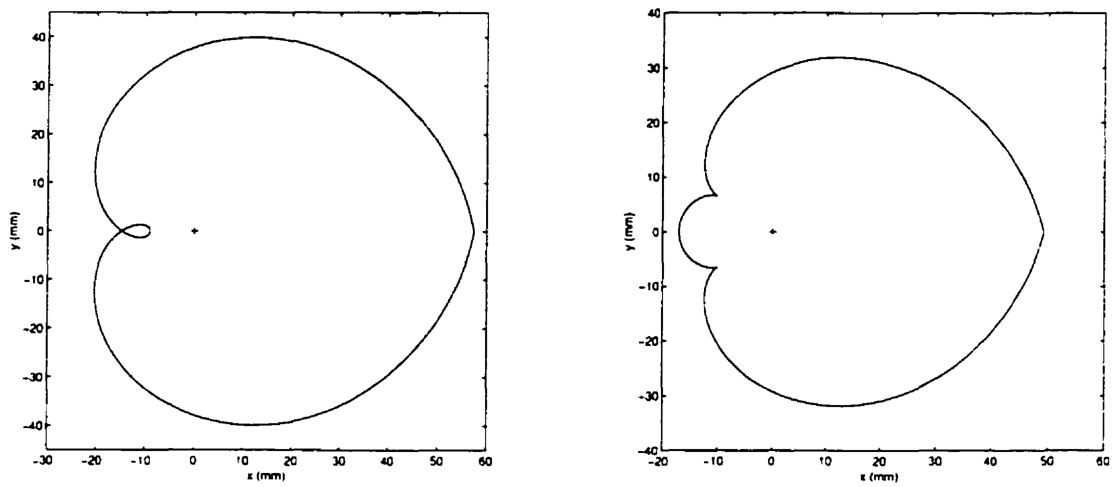

(a) (b)

FIGURE 4.1. An example of a pseudo-convex cam, generated with the parameters, $N = 5$, $r = 0.88$ and $a_1 = 75$mm: (a) the pseudo-convex pitch curve; (b) its cam profile

2. Undercutting Avoidance

Undercutting occurs when the follower or the cam cannot produce the desired path. This phenomenon happens when the radius of the roller is greater than or equal to the minimum absolute value of the radius of curvature of the pitch curve, i.e., when $1 - a_4\kappa_p \leq 0$

The condition on r that the planar Speed-o-Cam must satisfy to avoid undercutting, i.e., to ensure $1 - a_4\kappa_p > 0$ is (González-Palacios and Angeles, 1993, 1999)

$$r < \frac{1}{1 + 1/N} \tag{4.9}$$

$$r > \frac{1}{1 - 1/N} \tag{4.10}$$

where eqs.(4.9) and (4.10) are valid for external and internal Speed-o-Cam, respectively. Also note that $r < 1$ and, correspondingly, $r > 1$ for external and internal Speed-o-Cam, whence it is clear that r is bounded for external layouts as

$$0 < r < \frac{1}{(1 + 1/N)^2} \tag{4.11}$$

while, for internal layouts:

$$r > \frac{1}{(1 - 1/N)^2} \tag{4.12}$$

with N denoting the speed reduction of $N : 1$, which is an integer greater than unity.

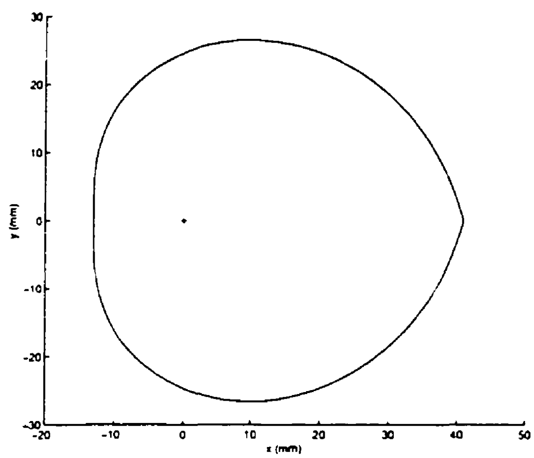

(a) (b)

FIGURE 4.2. Feasible convex cam profiles of external Speed-o-Cam: (a) for $N = 8$, with $r = 0.7901$ and $a_1 = 100$mm; (b) for $N = 5$, with $r = 0.6944$ and $a_1 = 75$mm

Intervals (4.11) and (4.12) ensure an acceptable fully-convex cam profile, for external and internal Speed-o-Cam, respectively. Four examples are shown in Figs. 4.2 and 4.3 to illustrate the convex cam profiles generated with various values of r and N. We select the value of r which yields the smallest maximum pressure angle of the mechanism.

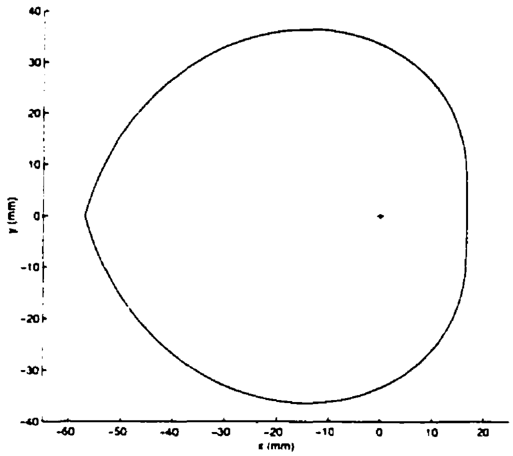

(a)

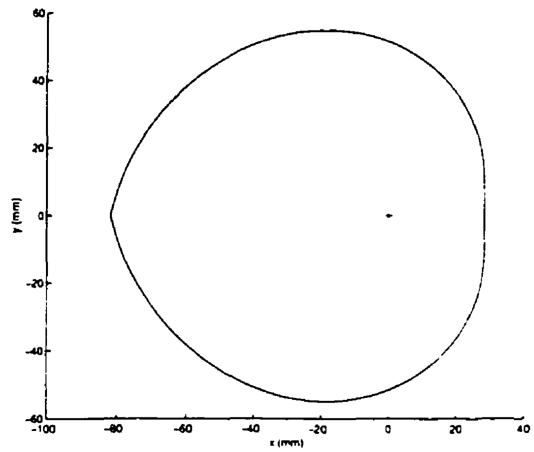

(b)

FIGURE 4.3. Feasible convex cam profiles of internal Speed-o-Cam: (a) for $N = 8$, with $r = 1.3061$ and $a_1 = 100$mm; (b) for $N = 5$, with $r = 1.5625$ and $a_1 = 100$mm

3. Pressure-Angle Constraints

The pressure angle μ of a cam is the angle between the line of motion of the follower $\mathcal{L}$ and the normal $\mathcal{N}$ to the cam surface at the point of contact between the cam and the follower, as depicted in Fig. 4.4. The force exerted on the follower by the cam acts along the common normal $\mathcal{N}$. We can resolve the contact force R into two components: $R\cos\mu$ is the force that actually drives the follower; $R\sin\mu$ is the component that is transmitted to the bearings of the follower. If $|\mu| = 30°$, then 50% of the force R will not drive the follower, but cause stresses on the follower bearings, which might result in rapid wear.

Therefore, to ensure good force transmission, the pressure angle is usually kept within $-30° < \mu < 30°$. A pressure angle expression for planar cam mechanisms is available in the literature (Angeles and López-Cajún, 1991; González-Palacios and Angeles, 1993; Rothbart, 1956; Tesar and Matthew, 1976), namely,

The value of r is selected for a minimum value of maximum pressure angle. Figure 4.5 shows the pressure angle plot for external Speed-o-Cam, with $r = 0.6944$

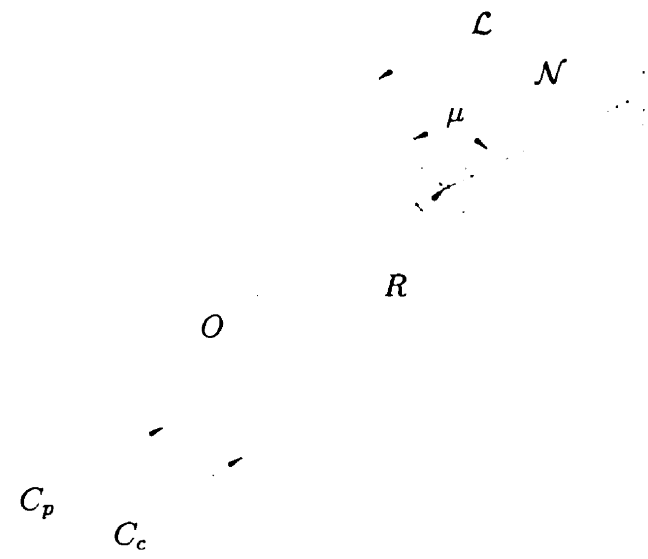

FIGURE 4.4. Pressure angle of an oscillating roller-follower cam mechanism

and $N = 5$ vs. ψ, of two conjugate cams. A similar procedure has been carried out for the cases of $N = 5$ and $N = 8$, with various values of r, as recorded in Tables 4.1–4.3.

$$\tan\mu = \frac{r(\phi' - 1) - \cos\phi}{\sin\phi}$$

It turns out that for both internal and external planar Speed-o-Cam, there is no solution which satifies both the convexity condition and the pressure angle bound within 30°. In consequence, we select the value of r which yields the minimum maximum pressure angle, namely, that which attains a minimum curvature of zero.

A performance measurement, termed *service factor* is introduced here to measure the percentage of the Speed-o-Cam working cycle within the acceptable pressure angle, i.e. $-30° < \mu < 30°$. In the case of a speed reduction of $5:1$, the value of r which gives the minimum curvature of zero is $r = 0.6944$, its service factor being found to be 85%, which is judged acceptable. However, in order to obtain an industrial standard bound of the service factor, tests have to be carried out to study

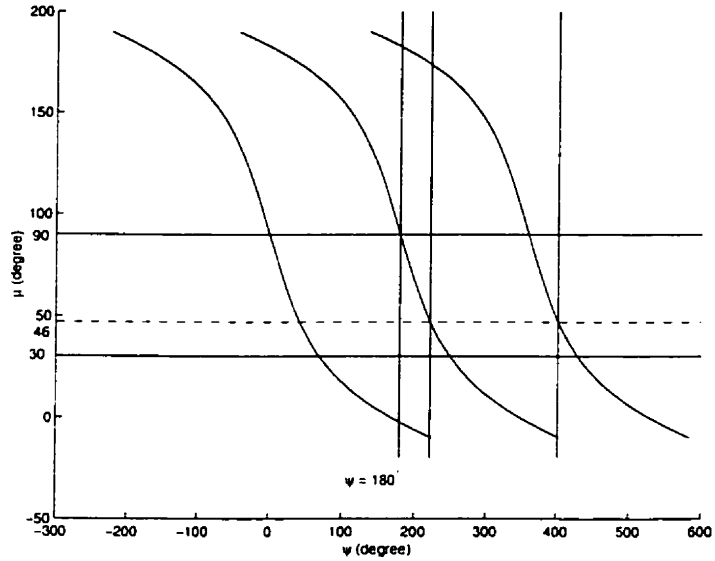

FIGURE 4.5. Pressure-angle distribution for external Speed-o-Cam of two conjugate cams with parameters $r = 0.6944$ and $N = 5$ vs. ψ

r	$\mu(^\circ)$
0.65	57.70
0.66	55.55
0.67	53.26
0.68	50.79
0.69	48.14
0.6944	46.92

TABLE 4.1. Pressure angle of external Speed-o-Cam for various values of r with $N = 5$

the performance of the mechanism because only experience can tell what ranges of this performance-index values are acceptable.

r	$\mu(°)$
0.782	47.83
0.784	47.11
0.786	46.39
0.788	45.63
0.79	44.87
0.7901	44.85

TABLE 4.2. Pressure angle of external Speed-o-Cam for various values of r with $N = 8$

r	$\mu(°)$
1.3062	42.69
1.31	43.36
1.32	45.07
1.33	46.70
1.34	48.29
1.35	49.79

TABLE 4.3. Pressure angle of internal Speed-o-Cam for various values of r with $N = 8$

CHAPTER 5

Dynamic Balancing of Planar Speed-o-Cam

Dynamic forces are, in general, time varying, exerted on the fixed frame by virtue of the inertia forces of moving parts in a machine, thereby imparting vibratory forces to the frame. This vibration and the accompanying noise can affect the machine performance and the structural integrity of the machine foundation. especially in high-speed machinery.

Unbalance due to rotating masses is referred to as rotating unbalance. which occurs in the case of Speed-o-Cam. This unbalance exerts a shaking force and moment onto the bearings mounted on the fixed frame and thus, affects the life of the bearings and hence, of the whole mechanism. To eliminate the unbalance force and moment, we apply a general procedure in balancing rotating machinery: static balancing and dynamic balancing.

Static unbalance is characterized by a net shaking force $\mathbf{f}_s$ and dynamic unbalance is characterized by a combination of a net shaking force and a net shaking moment, $\mathbf{m}_s$. Hence, in order to eliminate the unbalance in a cam mechanism, both the shaking force and the shaking moment must be equal to zero.

We analyze planar Speed-o-Cam in two parts: the low-speed shaft, which carries the follower and rollers, and the high-speed shaft, i.e., the camshaft, which carries the cams. It is obvious that both shafts are statically balanced because of symmetries. Therefore, the sections below will focus on the dynamic balancing of the two shafts.

1. Low-Speed Shaft

The low-speed shaft is formed by a follower and a set of rollers arranged in symmetric arrays. In consequence, the centre of mass of the low-speed shaft is on the axis of rotation, and hence, the low-speed shaft satisfies the static and dynamic balancing conditions, i.e.,

$$\mathbf{f}_s = \mathbf{0} \tag{5.1}$$

$$\mathbf{m}_s = \mathbf{0} \tag{5.2}$$

2. High-Speed Shaft

Consider a camshaft formed by two conjugate cams both rotated 180° and axially-translated one with respect to the other, which is the case in planar Speed-o-Cam. Since the centres of mass of the cams do not coincide with the axis of rotation, there exists a shaking moment normal to the shaft axis when the shaft rotates. Hence, the camshaft is statically balanced but dynamically unbalanced.

The basic idea in solving the unbalance problem is the redistribution of the mass, which involves removal or addition of mass, or a combination of both, from and to rotating machine members. To minimize the total mass of Speed-o-Cam, we attempt first material removal and then, material addition, as needed.

Since we are dealing with planar parts and, furthermore, a single material, the relationship between the area A and the mass m is simply

$$m = \rho t A$$

where ρ is the mass density of the material and t is the uniform thickness of the part. In the balance of the chapter, thus, we focus on area properties instead of mass properties.

2.1. Material removal. If the centre of mass of the cams can be moved such that it coincides with the axis of rotation of the cam, as in the case of the low-speed shaft, then the camshaft is dynamically balanced, i.e. the moment of the inertia forces of the cams in a direction normal to the axis of rotation vanishes. To achieve this, three circular holes, namely, C_2, C_3 and C_4, have been proposed to be drilled on the cam plate to translate the mass centre of the cam to the axis of rotation of the camshaft, if possible; otherwise, we attempt to shift this centre the nearest possible to that axis. The corresponding layout is shown in Fig. 5.1.

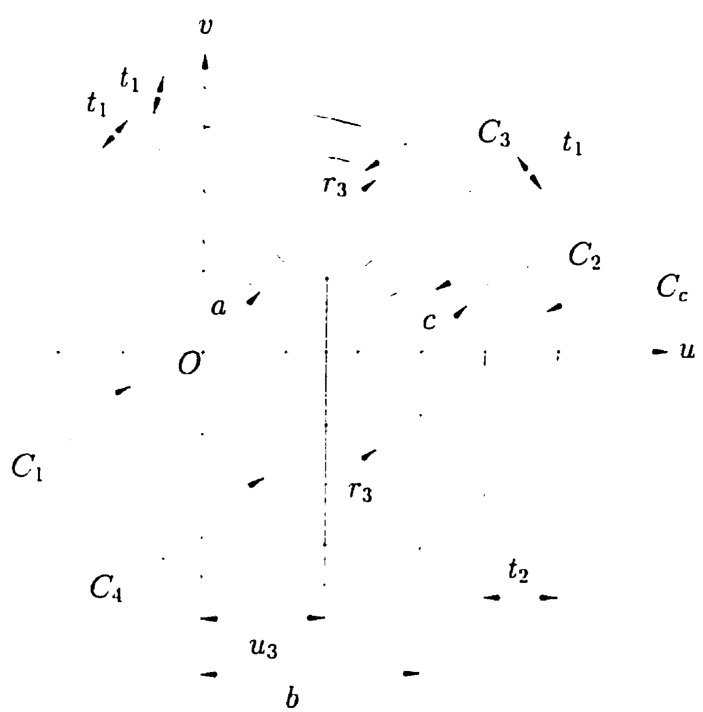

FIGURE 5.1. Cam plate with three holes drilled

Referring to Fig. 5.1, C_1 is the cross section of the camshaft; C_2 is a circular hole with its centre located on the u-axis so that the centre of mass of the cam is shifted only in the u-direction; C_3, which is the mirror image of C_4 about the u-axis, is also a circular hole, to be bored on the cam plate. Moreover, a, c and r_3 are the radii of C_1, C_2 and C_3, respectively, while b and u_3 are the distances from the centre of C_2 and C_3, to the origin O, i.e., the centre of the camshaft cross section, respectively.

We proceed below to derive a parametric model, of a particular choice of three holes bored, allowing us to decide on the values of the parameters that will yield a balanced cam plate: If we set the distance t_2 of Fig. 5.1 to lie within a range, then variables b and c are fixed by the geometry of the cam plate. Once the location of C_2, i.e. parameters b and c, are fixed, the centre P of circle C_3, shown in Fig. 5.2, is found by imposing the condition that C_3 is tangent to C_1 and C_2. Finally, the position of P is selected such that the distance d from the centre of C_3 to the cam profile C_o, illustrated in Fig. 5.2, be equal to R.

From Fig. 5.2, $R = r_3 + t_1$, whence the locus of P, which turns out to be the hyperbola L_P when $a \neq c$, satisfies the relations:

$$u^2 + v^2 = (a + R)^2 \tag{5.3}$$

$$(u - c)^2 + v^2 = (b + R)^2 \tag{5.4}$$

Solving eqs.(5.3) and (5.4) for u and v leads to:

$$u = \frac{2R(a - b) + a^2 + c^2 - b^2}{2c} \tag{5.5}$$

$$v = \pm\sqrt{Bu^2 + Cu + D} \tag{5.6}$$

with parameters B, C and D given by

$$B = \left(\frac{c}{a-b}\right)^2 - 1$$

$$C = c\left[1 - (\frac{c}{a-b})^2\right]$$

$$D = \frac{1}{4}\left\{(a-b)^2 + c^2\left[\left(\frac{c}{a-b}\right)^2 - 2\right]\right\}$$

In the case of $a = c$, the locus of P is a vertical line parallel to the v-axis, of equation $u = u_3$.

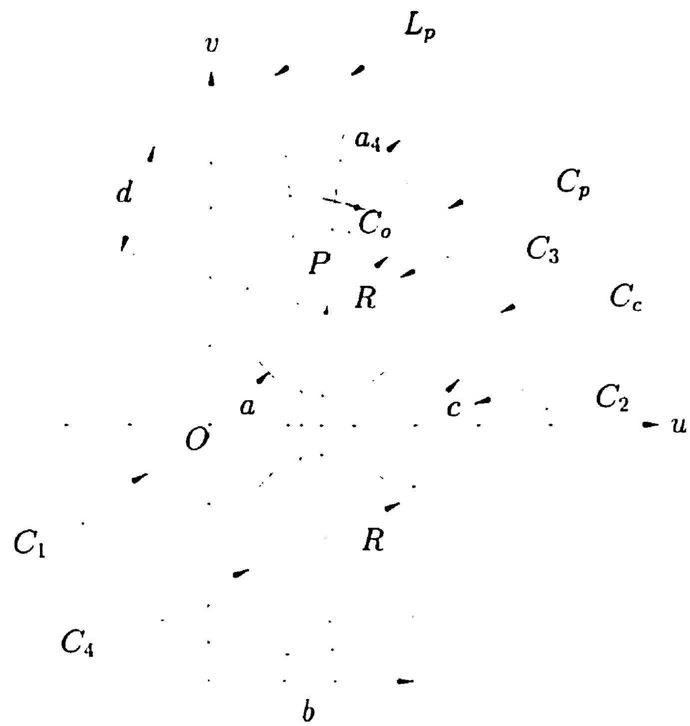

FIGURE 5.2. Cam plate designated for locus P

To obtain the distance d, we need the direction of the tangent or, equivalently, of the normal to the pitch curve. The parametric equations of the normal to any arbitrary curve $x = x(q)$, $y = y(q)$ at $q = q_o$ are given by (Bajpai, Mustoe and Walker, 1989)

$$x(t) = x(q_o) + t\frac{dy}{dq}(q_o) \tag{5.7}$$

$$y(t) = y(q_o) - t\frac{dx}{dq}(q_o) \tag{5.8}$$

where t is the parameter on the normal to the curve at $q = q_o$.

In our case, it is natural to use $q = \psi$, the parametric equations of the normal to the pitch curve $u_p(\psi)$, $v_p(\psi)$ at $\psi = \psi_o$ thus becoming

$$u(t) = u_p(\psi_o) + t\frac{dv_p}{d\psi}(\psi_o) \tag{5.9}$$

$$v(t) = v_p(\psi_o) - t\frac{du_p}{d\psi}(\psi_o) \tag{5.10}$$

Using eqs.(5.9) and (5.10), we obtain

$$v = Ku + L \tag{5.11}$$

where

$$\begin{aligned} K &= -\frac{du_p}{d\psi}(\psi_o)/\frac{dv_p}{d\psi}(\psi_o) \\ L &= v_p(\psi_o) - Ku_p(\psi_o) \end{aligned}$$

The intersection of the normal to the pitch curve and the hyperbola L_P at $\psi = \psi_o$ is obtained by substituing eq.(5.11) into eq.(5.6), i.e.,

$$u = \frac{C - 2KL \pm \sqrt{(2KL - C)^2 - 4(K^2 - B)(L^2 - D)}}{2(K^2 - B)} \tag{5.12}$$

Using eqs.(5.11) and (5.12), we obtain a set of points $\{P_i\}$ of coordinates (u_i, v_i) on the hyperbola L_P corresponding to every value of $(u_p(\psi), v_p(\psi))$ at $\psi = \psi_i$. Thus, the distance d is obtained as

$$d = \sqrt{(u_p(\psi) - u_i)^2 + (v_p(\psi) - v_i)^2} - a_4 \tag{5.13}$$

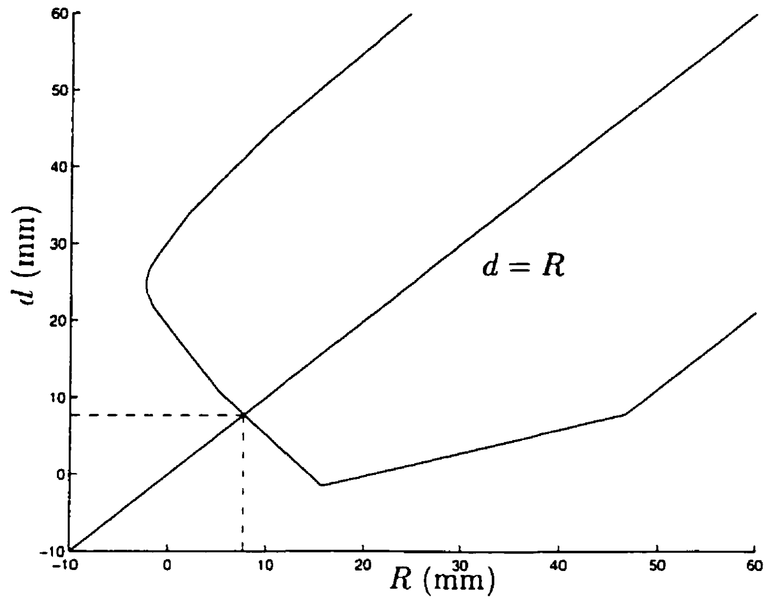

FIGURE 5.3. An example plot of d vs. R

To obtain the value of $d = R$, a graph of d vs. R is plotted, along with the line $d = R$, in Fig. 5.3. Their intersection gives the value of R sought. Once R is found, using eqs.(5.5) and (5.6), the location of P is determined. Figure 5.4 shows the cam profile created after applying this procedure with parameters $t_1 = 2$mm, $t_2 = 5$mm, $a = 9.5$mm, $b = 12.5$mm, $c = 12.5$mm and $d = 7.75$mm. Figure 5.5 shows the camshaft created using Pro/Engineer.

Now we recall that our intention of removing material from the cam plate is to shift the centroid of the cam plate to the axis of rotation, namely the axis perpendicular to the u and v axes through point O. Hence, we need to verify the location of the centroid of the new cam plate created.

2.1.1. *Centroid.* The centroid of a planar object composed of n given shapes of known centroids can be obtained using

$$u_{cm} = \sum_{i=1}^{n} \frac{A_i}{\sum_{j=1}^{n} A_j} u_i \quad \text{and} \quad v_{cm} = \sum_{i=1}^{n} \frac{A_i}{\sum_{j=1}^{n} A_j} v_i \tag{5.14}$$

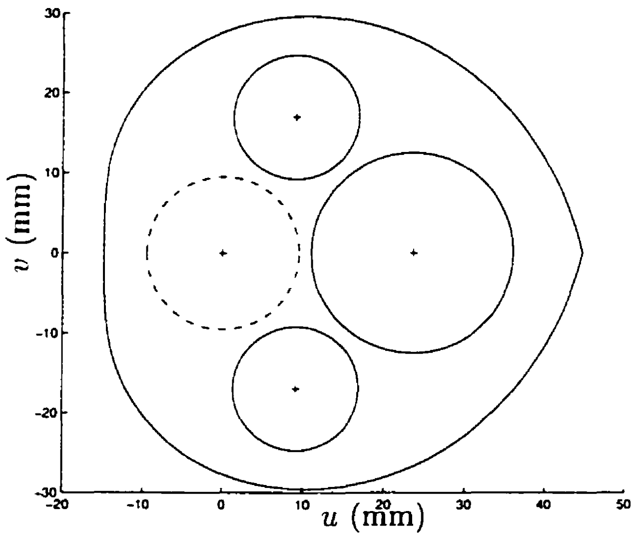

FIGURE 5.4. An example of a cam plate with three holes bored

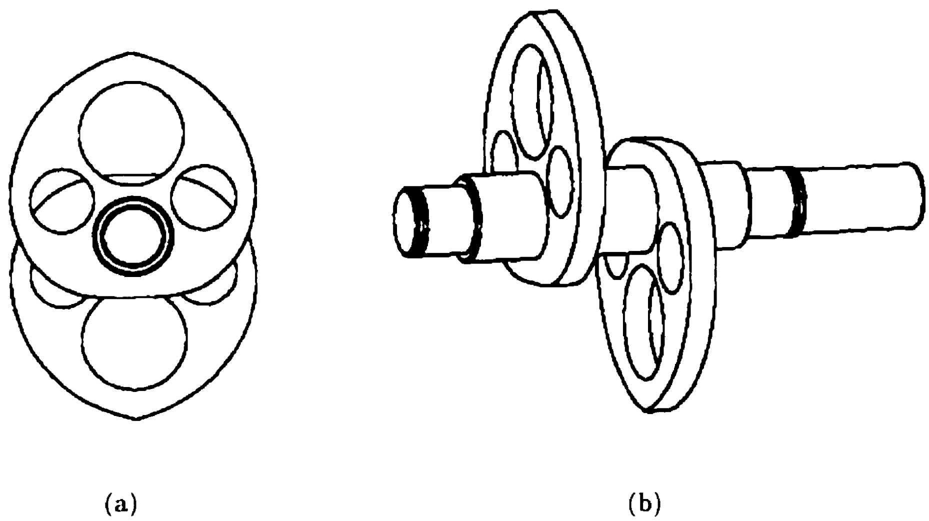

FIGURE 5.5. Camshaft created in Pro/Engineer: (a) side view; (b) perspective

where:

u_{cm} and v_{cm} : centre of mass of the object composed of n parts, in the u and v directions, respectively;

u_i and v_i : centre of mass of the ith part, in the u and v directions, respectively;

u_j and v_j : centre of mass of the jth part, in the u and v directions, respectively;

A_i : area of the ith part.

with $i = 1, 2, \cdots, n$ and $j = 1, 2, \cdots, n$.

From Fig. 5.1, due to the symmetry of the cam about the u-axis, $v_{cm} = 0$ and u_{cm} of the cam with removed material is found to be

$$u_{cm} = \frac{A_{\text{cam}} u_{\text{cam}} - A_2 u_2 - 2A_3 u_3}{A_c - A_2 - 2A_3} \tag{5.15}$$

where

A_{cam} : total area enclosed by the cam profile;

A_2 : area of circle C_2; $A_2 = \pi c^2$;

A_3 : area of circles C_3 and C_4; $A_3 = \pi r_3^2$;

u_{cam} : centroid abscissa of the cam plate;

u_2 : abscissa of the centre of C_2; $u_2 = b$;

u_3 : abscissa of the centre of C_3 and C_4.

To have the centroid coincide with the axis of rotation, we set $u_{cm} = 0$ in eq.(5.15) and solve for u_3, thereby obtaining

$$u_3 = \frac{A_{\text{cam}} u_{\text{cam}} - \pi b c^2}{2\pi r_3^2} \tag{5.16}$$

Choosing a proper set of values of u_2, u_3, r_2 and r_3, constrained by the geometry conditions will balance the camshaft. In the case of a 5 : 1 reduction in planar Speed-o-Cam, there is no feasible set of solutions that can balance the camshaft. Realize that the centre of mass of the new cam plate created u_{cm} is given by eq.(5.15), we proceed to adding counterweights to the camshaft.

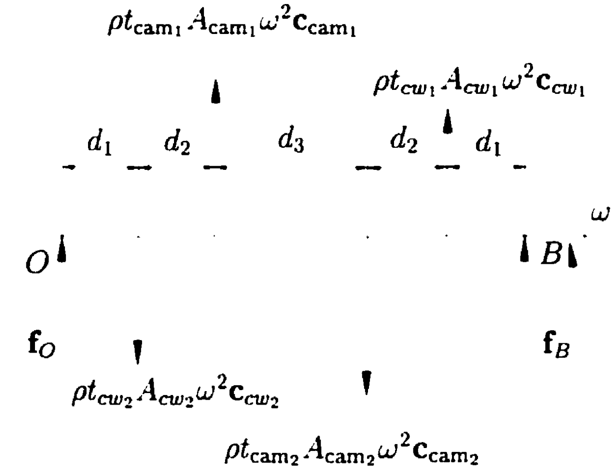

FIGURE 5.6. Free-body diagram of camshaft

2.2. Material addition. The notation used in Fig. 5.6 is described below:

A_{cw_1} and A_{cw_2}	:	the areas of the two counterweights;
A_{cam_1} and A_{cam_2}	:	the areas of the two conjugate cams;
t_{cw_1} and t_{cw_2}	:	the uniform thickness of the two counterweights;
t_{cam_1} and t_{cam_1}	:	the uniform thickness of the first and second cams;
$\mathbf{c}_1$ and $\mathbf{c}_2$	:	the position vectors of the centroids of the two counterweights;
$\mathbf{c}_{\mathrm{cam}_1}$ and $\mathbf{c}_{\mathrm{cam}_2}$	:	the position vectors of the centroids of the two cams;
ω	:	the constant angular velocity of the camshaft;
ρ	:	the mass density of the material of the camshaft.

Consider the force-balance and the moment-balance conditions, the latter taken with respect to point O, about the axis of rotation, namely,

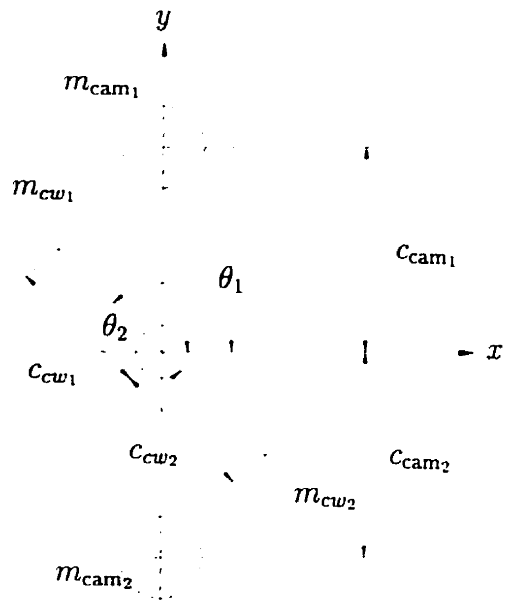

FIGURE 5.7. Diagram for moment balance

$$
\begin{aligned}
\mathbf{f}_s &= \rho t_{\text{cam}_1} A_{\text{cam}_1} \omega^2 \mathbf{c}_{\text{cam}_1} + \rho t_{\text{cam}_2} A_{\text{cam}_2} \omega^2 \mathbf{c}_{\text{cam}_2} + \rho t_{cw_1} A_{cw_1} \omega^2 \mathbf{c}_{cw_1} \\
&\quad + \rho t_{cw_2} A_{cw_2} \omega^2 \mathbf{c}_{cw_2} + \mathbf{f}_O + \mathbf{f}_B = \mathbf{0} \qquad (5.17) \\
\mathbf{m}_s &= \rho t_{cw_1} A_{cw_1} \omega^2 (d_1 + 2d_2 + d_3) \mathbf{c}_{cw_1} + \rho t_{\text{cam}_2} A_{\text{cam}_2} \omega^2 (d_1 + d_2 + d_3) \mathbf{c}_{\text{cam}_2} \\
&\quad + \rho t_{\text{cam}_1} A_{\text{cam}_1} \omega^2 (d_1 + d_2) \mathbf{c}_{\text{cam}_1} + \rho t_{cw_2} A_{cw_2} \omega^2 d_1 \mathbf{c}_{cw_2} = \mathbf{0} \qquad (5.18)
\end{aligned}
$$

Note that simplifications arise from the symmetric geometry of the camshaft:

$$
\mathbf{c}_{cw_1} = -\mathbf{c}_{cw_2} \quad , \quad \mathbf{c}_{\text{cam}_1} = -\mathbf{c}_{cam_2}
$$

$$
A_{cw_1} = A_{cw_2} \quad , \quad A_{\text{cam}_1} = A_{\text{cam}_2}
$$

Denote by c_{cw} the magnitude of $\mathbf{c}_{cw_1}$ and $\mathbf{c}_{cw_2}$; c_{cam} the magnitude of $\mathbf{c}_{\text{cam}_1}$ and $\mathbf{c}_{\text{cam}_1}$; $A_{cw} = A_{cw_1} = A_{cw_2}$ and $A_{\text{cam}} = A_{\text{cam}_1} = A_{\text{cam}_2}$. Substituting these parameters into eqs.(5.17) and (5.18), and referring to Fig. 5.7, we obtain, for the force-balance equation,

$$\mathbf{f}_O = -\mathbf{f}_B \tag{5.19}$$

and two scalar equations in x and y for the moment condition. For the x-component,

$$\begin{aligned} & t_{cw}A_{cw}(d_1 + 2d_2 + d_3)c_{cw}\cos\theta_1 + t_{\text{cam}}A_{\text{cam}}(d_1 + d_2 + d_3)c_{\text{cam}}\cos 270^\circ \\ & + t_{\text{cam}}A_{\text{cam}}(d_1 + d_2)c_{\text{cam}}\cos 90^\circ + t_{cw}A_{cw}d_1c_{cw}\cos\theta_2 = 0 \end{aligned} \tag{5.20}$$

where ρ has been deleted. After expansion, the above relation reduces to

$$t_{cw}A_{cw}(2d_2 + d_3)c_{cw}\cos\theta_1 = 0 \tag{5.21}$$

We obtain the y-component expression likewise:

$$A_{cw}t_{cw}(2d_2 + d_3)c_{cw}\sin\theta_1 - A_{\text{cam}}t_{\text{cam}}d_3c_{\text{cam}} = 0 \tag{5.22}$$

It follows that $\theta_1 = 90^\circ$ verifies eq.(5.21). Substituing this value of θ into eq.(5.22) leads to

$$c_{cw} = \frac{A_{\text{cam}}t_{\text{cam}}}{A_{cw}t_{cw}}\frac{d_3}{2d_2 + d_3}c_{\text{cam}} \tag{5.23}$$

For manufacturability purposes, circular counterweights are proposed since, as mentioned in Chapter 3, a circle is the most robust curve for a machine tool to follow. We introduce parameters a, e and f as defined in Fig. 5.8.

From Fig. 5.8, the centroid of the counterweight lies a distance f from O, in the $-y$ direction, i.e.,

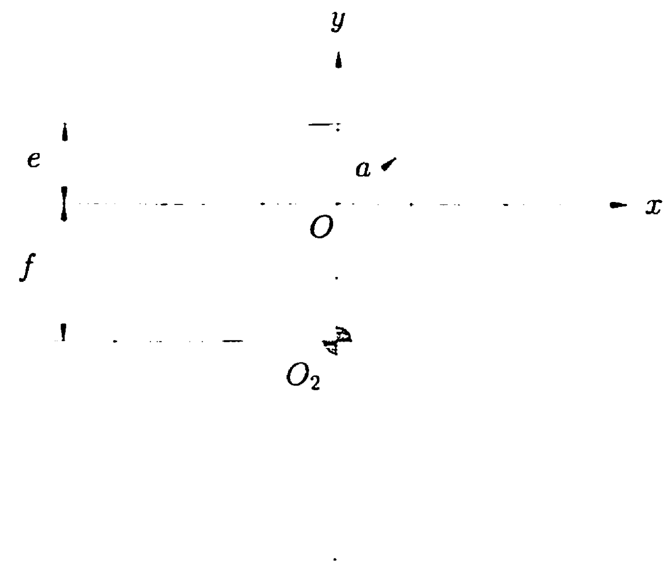

FIGURE 5.8. Circular counterweight proposed for planar Speed-o-Cam

$$c_{cw} = f \tag{5.24}$$

Apparently,

$$A_{cw} = \pi(e + f)^2 \tag{5.25}$$

With eqs.(5.23), (5.24) and (5.25), and taking into account the sign of the ordinate of O_2, we obtain a cubic equation to determine f:

$$f^3 + 2ef^2 + e^2 f - \frac{d_3 A_{\mathrm{cam}} t_{\mathrm{cam}} c_{\mathrm{cam}}}{\pi t_{cw}(2d_2 + d_3)} = 0 \tag{5.26}$$

It is apparent that having $e > a$ would lead to more unbalance, since this would be equivalent to adding material to the camshaft, a minimum value of e being preferred in this case. Choosing $e = a$ and using the maximum possible value of t_{cw}, we minimize the radius of the counterweight. With these constraints, the value of f can be readily computed.

For the case of a speed reduction of 5 : 1, we computed the counterweight parameters and created a solid model in Pro/Engineer, as displayed in Fig. 5.9 with the parameters $d_2 = 12.5$mm, $d_3 = 26$mm, $e = a = 19/2$mm, $t_{cam} = 6$mm, $t_{cw} = 8$mm, $c_{\text{cam}} = 12.0653$mm, $A_{\text{cam}} = 1.96 \times 10^6\text{mm}^2$ and $f = 8.6942$mm.

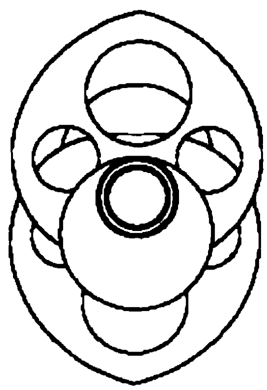

(a)

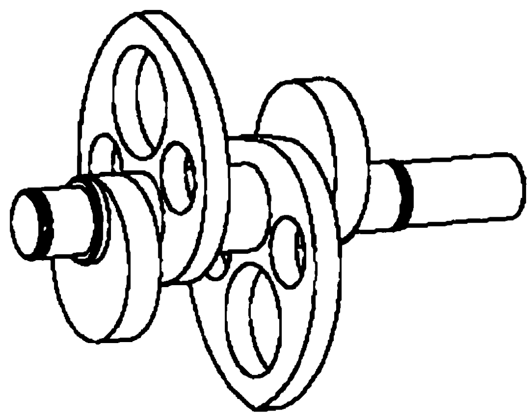

(b)

FIGURE 5.9. Camshaft with counterweights, created in Pro/Engineer: (a) side view; (b) perspective.

CHAPTER 6

Concluding Remarks

1. Conclusions

Design for manufacturability was the subject of this thesis; its principles were applied to the design of a planar speed-reducing cam mechanism. An index, termed machinability, was introduced to study the variability of the curvature of a profile. The Fourier analysis on the curvature of the profile was also undertaken, to study the frequency content of the proposed cam profiles. Both machinability and Fourier analysis indicate that the machining errors in CNC machine tools can be reduced by removing the concave parts in the cam profile. The convexity of the cam profile should lead to less noise or manufacturing error in machining the profile.

In consequence, a methodology for the design of a convex cam in a speed-reducer cam mechanism, specifically, planar Speed-o-Cam, for both external and internal layouts, was developed. The convexity of the cam profile was produced and the pressure angle was suitably bounded. It turned out that a convex cam plate with a pressure angle bounded by the industry-practice of 30° was not possible. We then devised a performance index, the service factor, that measures the percentage of a mechanism working cycle, in which the mechanism operates within acceptable pressure-angle bounds of ±30°. We found that the service factor of our design is 85%, which is thought to be acceptable. What a minimum service-factor value is acceptable is, of course, application dependent. Only experience can tell what minimum value of the service factor is accpetable for each application. This is an area for future research.

The balancing of the mechanism, aiming at minimizing the mass of the counterweights, was studied, a procedure to balance the camshaft having been devised. The work reported here targeted the performance and the life span of the mechanism, within the spirit of robust engineering, as propounded by Taguchi and his school.

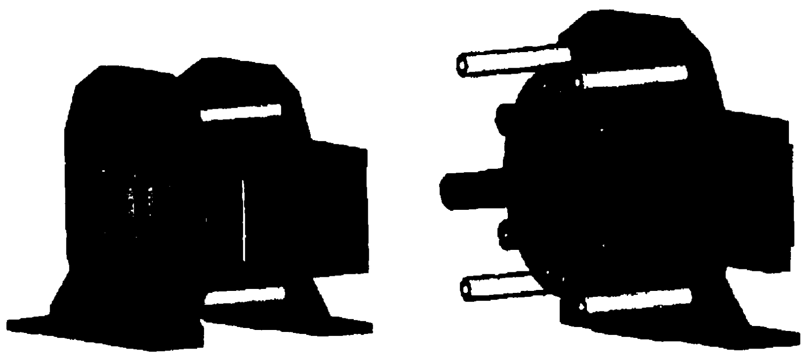

(a) (b)

FIGURE 6.1. New design of external planar Speed-o-Cam with $N = 5$ (a) perspective view; (b) details view

A model of external planar Speed-o-Cam with $N = 5$ was created using Pro/Engineer, as shown in Fig. 6.1; its animation was created using Pro/Engineer's module Pro/Mechanica.

2. Recommendations for Future Research

As an extension to the work reported here, further research is recommended, as follows:

(i) To formulate a mathematical model of a machine tool milling cam profiles. The relationship between the natural frequencies and the chattering effect of the machine tool, along with the response of the machine tool when cutting a workpiece might further explain the effect on manufacturability due to high curvature changes in the workpiece.

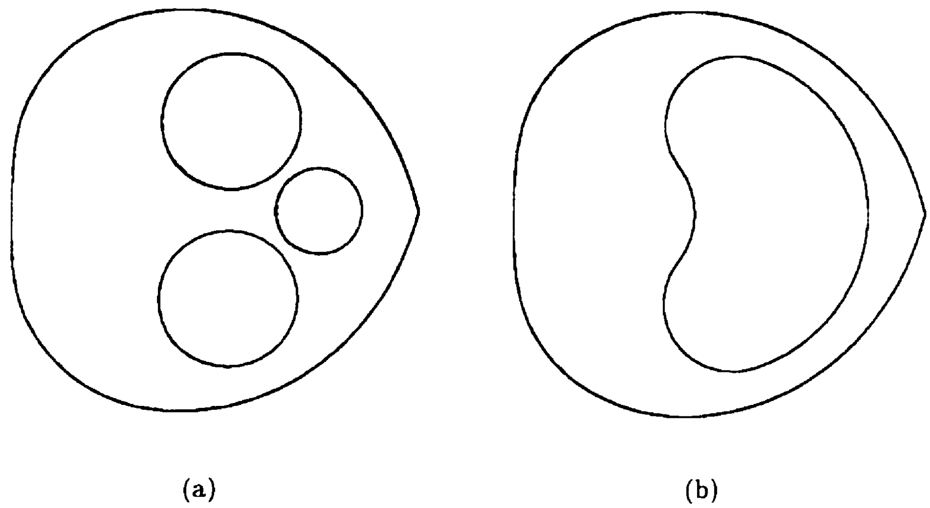

FIGURE 6.2. Cam plates bored with (a) three holes; (b) one noncircular hole

(ii) To improve the balancing of the camshaft. Instead of making three circular holes, we could remove the material from the cam plate by blending those three holes. This will lead to more material removal and the counterweight might be eliminated from the design. However, the structural behaviour of a light cam plate should be given due consideration. Figure 6.2 shows a contrast of the cam plates with three circular bores and with a single, noncircular bore.

(iii) To improve the pressure-angle distribution by using three conjugate cams located 120° from one another, instead of only two. The maximum pressure angle is expected to reduce tremendously for three conjugate cams, and hence, a higher speed reduction of the mechanism should be possible.

(iv) To further investigate the feasibility of the cascading of two or more Speed-o-Cam mechanisms to obtain much higher speed reductions, of the order of $100,000 : 1$, as required by modern machinery, e.g., computer disk drives.

(v) To investigate epicyclic trains of cam-roller speed reducers.

(vi) To conduct experimental work on the use of the concept of machinability with the aim of introducing it as an industry standard for precision machining.

(vii) To experimentally devise industry standards for classes of applications, with regard to the concept of service factor.

REFERENCES

ANGELES, J. and LÓPEZ-CAJÚN, C.S., 1991, *Optimization of Cam Mechanisms*, Kluwer Academic Publishers, Dordrecht, Boston.

BAJPAI, A.C., MUSTOE, L.R. and WALKER, D., 1989, *Engineering Mathematics*, Second Edition, John Wiley & Sons, Chichester [England], New York.

BESANT, C.B., 1983, *Computer-Aided Design and Manufacture, Second Edition*, Chichester [West Sussex] : Ellis Horwood ; New York : Halsted Press.

BRALLA, J.G., 1999, *Design For Manufacturability Handbook*, Second Edition, McGraw-Hill Book Co., New York.

CHEN, F.Y., 1982, *Mechanics and Design of Cam Mechanisms*, Pergamon Press, New York.

DARLOW, M.S., 1989, *Balancing of High-Speed Machinery*, Springer-Verlag, New York.

DENAVIT, J. and HARTENBERG, R.S., 1964, *Kinematic Synthesis of Linkages*, McGraw-Hill Book Co., New York ; Toronto.

GONZÁLEZ-PALACIOS, M.A. and ANGELES, J., 1993, *Cam Synthesis*, Kluwer Academic Publishers, Dordrecht, Boston.

GONZÁLEZ-PALACIOS, M.A. and ANGELES, J., 1999, "The Design of a Novel Mechanical Transmission for Speed Reduction", *ASME Journal of Mechanical Design*, Vol. 121, pp. 538–543.

HAMMING, R.W., 1962, *Numerical Methods for Scientists and Engineers*, McGraw-Hill Book Co., New York.

HIRSCHHORN, J., 1962, "Pressure angle and minimum base radius", *Machine Design*,

JAMES, J.F., 1995, *A Student's Guide to Fourier Transforms: With Applications in Physics and Engineering*, Cambridge University Press, Cambridge ; New York.

LIN, S.C., 1994, *Computer Numerical Control, From Programming to Networking*, Delmar Publishers, New York.

MALIK, A.K., GHOSH, A. and DITTRICH, G., 1994, *Kinematic Analysis and Synthesis of Mechanisms*, CRC Press, Boca Raton.

NAVARRO-MARTÍNEZ, O.R., WU, C.-J. and ANGELES, J., 2001, "The size-minimization of planar cam mechanisms", *Mechanism and Machine Theory*, Vol. 36, pp. 371–386.

NORTON, R.L., 1999, *Design of Machinery: An Introduction to the Synthesis and Analysis of Mechanisms and Machines*, WCB/McGraw-Hill Book Co., Boston; London.

RAMIREZ, R.W., 1985, *The FFT Fundamentals and Concepts*, Prentice-Hall, Englewood Cliffs, New Jersey.

ROSS, P.J., 1996, *Taguchi Techniques for Quality Engineering: Loss Function, Orthogonal Experiments, Parameter and Tolerance Design*, McGraw-Hill Book Co., New York.

ROTHBART, H.A., 1956, *Cams: Design, Dynamics, and Accuracy*, John Wiley and sons Inc., New York.

TAGUCHI, G., 2000, *Robust Engineering*, McGraw-Hill Book Co., New York.

TAGUCHI, G., 1988, "The development of quality engineering", *The ASI Journal*, Dearbon, MI, Vol. 1, No. 1.

TAYLOR, A.E., 1985, *General Theory of Functions and Integration*. Dover Publications, New York.

TESAR, D. and MATTHEW, G.K., 1976, *The Dynamic Synthesis, Analysis, and Design of Modeled Cam Systems*, Lexington Books, Lexington (Massachusetts).

TOBIAS, S.A., 1965, *Machine-Tool Vibration*, Blackie and Son Ltd., London.

VELDKAMP G.R., 1976, "On the Use of Dual Numbers, Vectors and Matrices in Instantaneous, Spatial Kinematics", *Mechanism and Machine Theory*, Vol. 11, pp. 141–156.

WELBOURN, D.B. and SMITH, J.D., 1970, *Machine-Tool Dynamics : An Introduction*, Cambridge University Press, London.

WILDE, D., 1991, "A counterexample to signal-to-noise ratio as a measure of design robustness", DE-Vol. 32-1, *Advances in design automation*, Vol. 1, ASME.

WILSON, C.E. and SADLER, J.P., 1993, *Kinematics and Dynamics of Machinery*, Harper Collins College Publishers, New York.

WU, Y. and WU, A., 2000, *Taguchi Methods for Robust Design*, ASME Press, New York.

Document Log:

Manuscript Version 1 — April, 2001

Typeset by $\mathcal{A}\mathcal{M}\mathcal{S}$-LaTeX — 2 May 2001

MERN KEAT LEE

CENTRE FOR INTELLIGENT MACHINES, MCGILL UNIVERSITY, 3480 UNIVERSITY ST., MONTRÉAL (QUÉBEC) H3A 2A7, CANADA, *Tel.* : (514) 845-4238

E-mail address: mlee@cim.mcgill.ca

Typeset by $\mathcal{A}\mathcal{M}\mathcal{S}$-LaTeX